

Subcellular distribution of human RDM1 protein isoforms and their nucleolar accumulation in response to heat shock and proteotoxic stress

Lydia Messaoudi¹, Yun-Gui Yang¹, Aiko Kinomura², Diana A. Stavreva³,
Gonghong Yan¹, Marie-Line Bortolin-Cavaillé⁴, Hiroshi Arakawa⁵,
Jean-Marie Buerstedde⁵, Pierre Hainaut¹, Jérôme Cavaillé⁴, Minoru Takata² and
Eric Van Dyck^{1,*}

¹International Agency for Research on Cancer (IARC), 150 Cours Albert Thomas, 69372 Lyon, France, ²Department of Human Genetics, Research Institute for Radiation Biology and Medicine, Hiroshima University, 1-2-3 Kasumi, Minami-Ku, Hiroshima, Japan 734-8553, ³Laboratory of Receptor Biology and Gene Expression, Center for Cancer Research, National Cancer Institute, Bethesda, Maryland 20892, USA, ⁴Laboratoire de Biologie Moléculaire des Eucaryotes, LBME-CNRS UMR 5099 - IFR 109, Université Paul Sabatier, 118, Route de Narbonne, 31062 Toulouse, France and ⁵Institute for Molecular Radiobiology, GSF, Ingolstaedter Landstrasse 1, D-85764 Neuherberg-Munich, Germany

Received June 13, 2007; Revised August 28, 2007; Accepted September 11, 2007

Accession No. EF488473-EF488482

ABSTRACT

The *RDM1* gene encodes a RNA recognition motif (RRM)-containing protein involved in the cellular response to the anti-cancer drug cisplatin in vertebrates. We previously reported a cDNA encoding the full-length human RDM1 protein. Here, we describe the identification of 11 human cDNAs encoding RDM1 protein isoforms. This repertoire is generated by alternative pre-mRNA splicing and differential usage of two translational start sites, resulting in proteins with long or short N-terminus and a great diversity in the exonic composition of their C-terminus. By using tagged proteins and fluorescent microscopy, we examined the subcellular distribution of full-length RDM1 (renamed RDM1 α), and other RDM1 isoforms. We show that RDM1 α undergoes subcellular redistribution and nucleolar accumulation in response to proteotoxic stress and mild heat shock. In unstressed cells, the long N-terminal isoforms displayed distinct subcellular distribution patterns, ranging from a predominantly cytoplasmic to almost exclusive nuclear localization, suggesting functional differences among the RDM1

proteins. However, all isoforms underwent stress-induced nucleolar accumulation. We identified nuclear and nucleolar localization determinants as well as domains conferring cytoplasmic retention to the RDM1 proteins. Finally, RDM1 null chicken DT40 cells displayed an increased sensitivity to heat shock, compared to wild-type (wt) cells, suggesting a function for RDM1 in the heat-shock response.

INTRODUCTION

The RNA recognition motif (RRM) is a widespread nucleic acid-binding domain of about 90 aa that displays a conserved protein fold and, with the exception of two small peptide motifs involved in RNA interaction (RNPI and RNP2), a great variability in sequence (1). Although RRM domains are encountered primarily in RNA-binding proteins, their targets are not restricted to RNA. Thus, some RRMs have been shown to bind single-stranded (ss) DNA (2–4) or double-stranded (ds) DNA (5–8), or even to mediate protein–protein interactions (9,10). RRM-containing proteins tend to have a modular structure consisting of one or multiple copies of the RRM, in association with other protein domains, such as the

*To whom correspondence should be addressed. Tel: +33 4 72 73 83 93; Fax: +33 4 72 73 83 22; Email: vandyck@iarc.fr or Vandyckeric@hotmail.com
Present address:

Lydia Messaoudi, Institut de Cancérologie Gustave Roussy, Villejuif, France

Yun-Gui Yang, Cancer Research UK, London Research Institute, Clare Hall Laboratories, UK

Gonghong Yan, Department of Pharmacology, University of Pittsburgh School of Medicine, USA

Minoru Takata, Radiation Biology Center, Kyoto University, Kyoto, Japan

arginine-serine-rich (RS) domain found in the serine-arginine (SR) protein family of splicing factors (11,12), or the arginine-glycine-rich (RGG) domain found, for instance, in nucleolin (13) and some heterogeneous nuclear ribonucleoproteins (hnRNPs) (14). These auxiliary domains have been shown to act as protein-protein interaction modules (15,16), participate in the interaction with RNA (17) and/or contribute to the intracellular localization of the protein (18–24). RRM-containing proteins display a wide subcellular distribution that reflects both the variety and multiplicity of their targets and their essential participation in processes such as transcriptional regulation, RNA splicing, editing and processing, RNA export, sequestration, transport, translation and stability, chromatin and telomere metabolism. In line with some of these activities, trafficking between intracellular and/or intranuclear compartments has been reported for several RRM-containing proteins, illustrating a highly dynamic and regulated subcellular distribution (25,26).

Recently, we identified a novel RRM-containing protein in vertebrates. Disruption of the *RDM1* gene (for *RAD52 Motif 1*) encoding this protein in the chicken B cell line DT40 resulted in an increased sensitivity to the anti-cancer drug cisplatin (27). Using gel-shift assays and electron microscopy, we showed that purified, recombinant RDM1 binds RNA and ssDNA, as well as dsDNA on which it assembles filament-like structures (27,28). RDM1 was also able to recognize distortions of the double helix caused by cisplatin-DNA adducts *in vitro*. The primary sequence of RDM1 revealed a single, N-terminal RRM but none of the auxiliary domains that are known to be associated with this motif. However, the RRM domain of RDM1 is followed by a short region, named RD motif, which is conserved in the DNA recombination and repair protein, RAD52 (27). In RAD52, the region comprising this motif plays an essential role in ssDNA binding (29). Biochemical analysis of a chicken RDM1 variant mutated in its RD motif revealed altered ssDNA-binding activity (28). Based on these observations, we proposed a role for the RD motif of RDM1 as a modulator of its RRM. To date, the biological targets and function of RDM1 remain unknown.

We previously reported the identification of a human cDNA encoding a 284-aa ORF corresponding to the full-length RDM1 protein (27). In this report, we undertook a reverse transcriptase (RT)-PCR analysis of *RDM1* expression. We describe the identification of eleven cDNAs encoding RDM1 isoforms. This extensive repertoire is generated by alternative pre-mRNA splicing and differential usage of two translational start sites, resulting in proteins with long or short N-terminus and a great diversity in the exonic composition of their C-terminus. By using tagged proteins and fluorescent microscopy, we examined the subcellular distribution of full-length RDM1, which was renamed RDM1 α , and some of long N-terminal isoforms. We found that RDM1 α undergoes subcellular redistribution and nucleolar accumulation in response to proteotoxic stress and mild heat shock. In the absence of stress, the long

N-terminal isoforms displayed distinct patterns of subcellular distribution, ranging from a predominantly cytoplasmic to an almost exclusive nuclear localization. However, all isoforms underwent stress-induced nucleolar accumulation. We identified nuclear and nucleolar localization determinants as well as domains conferring cytoplasmic retention to the RDM1 proteins, thus providing a structural basis for the diversity of their subcellular localizations. Finally, we report that *RDM1* null chicken DT40 cells exhibit an increased sensitivity to heat shock, compared to wild-type (wt) cells, suggesting a novel function for *RDM1* in the heat-shock response.

MATERIALS AND METHODS

Reagents and antibodies

Lactacystin and MG132 were from Calbiochem. Cycloheximide, actinomycin D, α -amanitin and leptomycin B were from Sigma. Oligonucleotides were purchased from Invitrogen or Eurogentec. DRAQ5 was from ALEXIS Biochemicals. The following antibodies were used: mouse anti-Flag (M2) monoclonal antibody (Stratagene), mouse anti-c-myc (clone 9E10) monoclonal antibody (Sigma), mouse anti-PML (PG-M3) monoclonal antibody (Santa Cruz), mouse anti-coilin (clone p δ) monoclonal antibody (Sigma), rabbit anti-nucleolin (abcam, ab22758), tetramethyl rhodamine isothiocyanate (TRITC)- and fluoresceine isothiocyanate (FITC)-conjugated anti-rabbit and anti-mouse, affinity-purified antibodies (Jackson ImmunoResearch Laboratories).

Plasmid construction, site-directed mutagenesis and cloning of RDM1 isoforms

The primers used for this study are listed in Supplementary Table 1. The human full-length RDM1 α ORF was PCR-amplified from a human testis cDNA library using primers EV041 and EV042 incorporating the ATG and stop codons, respectively, as well as restriction sites to facilitate cloning. The PCR fragment was digested with EcoRI and XhoI and cloned into the EcoRI/XhoI sites of pBluescript II SK (Stratagene) to generate pYG019. To construct pRDM1 α -EGFP, the RDM1 α ORF was PCR-amplified from pYG019 using primers EV061 and EV062, digested with XhoI and BamHI, and cloned into the XhoI/BamHI sites of pEGFP-N3 (BD Biosciences). To create pRDM1 α -mRFP, the BamHI/NotI fragment containing EGFP from pRDM1 α -EGFP was replaced with a BamHI/NotI fragment containing monomeric red fluorescent protein (mRFP) from pcDNA3-mRFP (30), and in-frame fusion was restored by site-directed deletion of the G present between the BamHI site and the ATG of mRFP in pcDNA3-mRFP. pEGFP-RDM1 α was created by subcloning a BamHI-ApaI fragment from pYG019 into the BglII/ApaI sites of pEGFP-C1 (BD Biosciences). To construct pFlag-RDM1 α , the RDM1 α fragment amplified with EV041 and EV042 was digested with NdeI, followed by end-blunting with the Klenow fragment of *Escherichia coli* DNA polymerase I in the presence of dNTPs, digestion with XhoI and cloning into the HpaI/

XhoI sites of pcDNA3-Flag. To generate pRDM1 α -myc, the RDM1 α ORF was amplified using primers EV061 and EV062, followed by cloning into the XhoI/BamHI sites of pcDNA3.1/myc-His(-)A (Invitrogen). To construct pEGFP-RDM1₉₀₋₂₈₄, a RDM1 α fragment was PCR-amplified with primers EV280 and EV281, digested with XhoI and BamHI and cloned into the XhoI/BamHI sites of pEGFP-C1. pEGFP-RDM1₉₀₋₁₃₃ was created by digesting pEGFP-RDM1₉₀₋₂₈₄ with HindIII and BamHI to remove sequences corresponding to exons 4–7, followed by end-blunting and self-ligation of the gel-purified plasmid. pEGFP-RDM1 α - Δ E3, lacking all of exon3, was constructed by PCR-based deletion, using primers EV295 and EV281, as well as the complementary primers EV293 and EV294 which overlap exons 2 and 4. The resulting fragment was cloned into the XhoI/BamHI sites of pEGFP-C1. pEGFP-RDM1₁₃₃₋₂₈₄ was created by cloning of a RDM1 α fragment amplified with primers EV304 and EV281 into the XhoI/BamHI sites of pEGFP-C1. pEGFP-RDM1₁₋₉₂ was created by digesting pEGFP-RDM1 α - Δ E3 with HindIII and BamHI to remove exons 4–7, followed by end-blunting and self-ligation of the gel-purified plasmid. To create pRD_{RDM1}-EGFP, the RD motif of RDM1 was PCR-amplified using primers EV300 and EV301, followed by cloning into the XhoI/BamHI sites of pEGFP-N3.

Site-directed mutagenesis of exon 3 in pEGFP-RDM1₉₀₋₁₃₃ was carried out with the mutagenic primer pairs EV296-EV297 (Y₁₂₀YF-AAA) or EV298-EV299 (R₉₈HK-AAA) using the QuickChange Site-Directed Mutagenesis kit from Stratagene. The isoforms of RDM1 containing long or short N-terminal sequences were amplified by RT-PCR on total RNA from HEK293T cells using primers EV061 and EV281, or EV254 and EV042, respectively. Following gel-purification and digestion with XhoI and BamHI, the bands were cloned into the XhoI/BamHI sites of pEGFP-C1. All constructs were confirmed by sequencing. The nucleotide sequences of the RDM1 isoforms have been submitted to the GenBankTM/DDBJ/EBI data bank with accession numbers EF488473-EF488482.

Fibrillarin-RFPCherry was generated by replacing the GFP in Fibrillarin-GFP (31) by a RFPCherry KpnI/BamHI fragment generated by PCR from RFPCherry in pRSETB vector (kind gift from Dr R.Y. Tsien, University of California, San Diego, CA).

Human cell culture and transfection

HEK293, HEK293T, HeLa and MCF7 cells were maintained in Dulbecco's modified Eagle's medium (DMEM) supplemented with 10% foetal bovine serum (FBS), 1 mM sodium pyruvate, 2 mM L-glutamine, penicillin and streptomycin (Gibco-BRL). Cells were maintained in a 5% CO₂ atmosphere at 37°C. For some experiments, cells were grown in CO₂-independent medium (Invitrogen) supplemented with 10% FBS and 4 mM L-glutamine. Cells were transiently transfected using Superfect (Qiagen), or FuGENE 6 (Roche). Stable pools of HEK293 clones expressing RDM1 α -EGFP and EGFP-RDM1 α were obtained following transfection with pEGFP-RDM1 α

and pEGFP-RDM1 α , respectively, using Effectene (Qiagen), and selection with G418 (1 mg/ml)(InvivoGen). Isolated clones were further purified by serial dilutions.

For localization experiments with Fibrillarin-RFPCherry, HeLa cells were transfected with both pRDM1 α -EGFP and Fibrillarin-RFPCherry by electroporation (electroporator ECM 830; BTX), using 7 μ g plasmid DNA and 15 μ g sheared salmon sperm carrier DNA in a 2 mm gap cuvette containing 10⁴ cells in a final volume of 200 μ l, at 200 V, 1 ms pulse, four pulses and 0.5 s intervals. After electroporation, the cells were grown overnight on 22 mm square coverslips each deposited on the bottom of a six-well plate, followed by treatment with MG132 and processing for confocal microscopy as described further.

Proteotoxic stress, heat shock and inhibition of transcription

HeLa or HEK293T cells were treated with lactacystin (10 μ M) or MG132 (10 or 25 μ M) for the indicated time. Heat stress was applied to cells grown in CO₂-independent medium by incubation at 43°C for 30 min in a water bath as described by Chatterjee and Fisher (32). For specific transcriptional inhibition of RNA pol I, or for inhibition of both RNA pol I and pol II, cells were treated for 2 h with 50 ng/ml (33) or 5 μ g/ml (34) actinomycin D, respectively. For specific inhibition of RNA pol II, 50 μ g/ml α -amanitin were added to the cells for 5 h (35).

Chicken DT40 cell culture and survival assays

DT40 cell culture was done as previously described (36). The analysis of cell survival following heat-shock treatment was carried out using colony formation assays, by plating serially diluted, heat-stressed cells in complete medium containing 1.4% methylcellulose followed by incubation at 39.5°C. Colonies were counted at ~10 days after plating. Cell survival following exposure to MG132 was determined by FACS analysis using a FACSCalibur (Becton Dickinson). Cells were stained with propidium iodide (PI) without fixation, and dead cells were defined as PI-positive cells.

Immunofluorescence and microscopy

Cells were seeded in chambered cover glasses (Lab-Tek) 16–20 h after transfection, and used in experiments ~48 h following transfection. For direct immunofluorescence analysis, cells were fixed with 2% paraformaldehyde in PBS for 15 min at room temperature and washed three times with PBS, and the cell nuclei were counterstained with DRAQ5 (1/5000 in PBS) for 5 min. For indirect immunofluorescence, cells were fixed with 2% paraformaldehyde in PBS for 15 min, permeabilized for 5 min in 0.2% Triton X-100 in PBS, and then blocked in PBS containing 0.1% FBS, 1% BSA and 0.2% Triton X-100 for 1 h at room temperature or overnight at 4°C. Cells were then incubated with the indicated primary antibodies (diluted in PBS containing 0.1% FBS, 1% BSA and 0.2% Triton X-100) for 1 h 45 min at room temperature, rinsed three times with 0.05% Tween 20 in PBS and incubated with TRITC- or FITC-conjugated

secondary antibodies for 45 min at room temperature. Cells were then rinsed twice with 0.05% Tween 20 in PBS, followed by counterstaining of the cell nuclei with DRAQ5 as described above. Primary antibodies were used at the following dilutions: 1:2000 (anti-nucleolin), 1:1000 (anti-Flag), 1:500 (anti-c-myc), 1:125 (anti-coilin), 1:100 (anti-PML). Secondary antibodies were used at a 1:200 (anti-mouse) or 1:1000 (anti-rabbit) dilution. Confocal microscopy was carried out using a Zeiss LSM510 laser scanning microscope.

For the visualization of HeLa cells expressing pRDM1 α -GFP and Fibrillarin-RFPCherry, control or MG132-treated cells were fixed in 3.5% paraformaldehyde at room temperature for 15 min. Cells were then washed with PBS three times for 10 min before final mounting in Vectashield mounting medium containing DAPI (Vector Laboratories, Inc.). Cells were observed using ZeissMeta confocal microscope with a 100 \times 1.3 N.A. oil immersion objective lens.

For the visualization of nucleolar RNA, control or MG132-treated HeLa cells were incubated with the RNA-selective fluorescent probe F22 (10 μ M) (37) for 20 min at 37 $^{\circ}$ C. Cells were then fixed in 3.5% paraformaldehyde and prepared for microscopy as described above. RNA staining of HEK293T cells was carried out by incubating paraformaldehyde-fixed cells with F22 (5 μ M) for 20 min at room temperature.

RNA extraction and RT-PCR analysis

Total RNA was extracted using the TRIzol reagent according to the manufacturer's instructions (Invitrogen), and reverse transcribed with SuperScript II Reverse Transcriptase (Invitrogen). *RDM1* cDNAs were amplified with the indicated primers. For semiquantitative RT-PCR analysis of *RDM1* expression, its cDNAs were co-amplified with β -actin (primers F-actin and R-actin). The PCR reaction mixture was denatured for 5 min at 94 $^{\circ}$ C, cycled 35 times (94 $^{\circ}$ C, 30 s; 61 $^{\circ}$ C, 30 s; 72 $^{\circ}$ C, 1 min), followed by a 7 min extension at 72 $^{\circ}$ C.

RESULTS

Identification of isoforms of human RDM1

We have previously reported the identification, from testis and brain cDNA libraries, of a human cDNA encoding a 284-aa ORF corresponding to the full-length RDM1 protein (27). This ORF is encoded by seven exons varying in size between 86 and 360 nt and interrupted by introns between 376 and 4438 nt long (see Supplementary Tables 2 and 3 for the coordinates of the *RDM1* ORF on chromosome 17 and its exon/intron organization, respectively). Preliminary RT-PCR analyses using primers designed to amplify the complete *RDM1* ORF from a variety of tissues and cell lines suggested the expression of isoforms arising from alternative splicing (data not shown, see also below). Limited evidence for alternative splicing of *RDM1* pre-mRNA was also reported in the AceView annotations of the National Center for Biotechnology Information (NCBI) human genome database (<http://www.ncbi.nih.gov/IEB/Research/Acembly/index.html>).

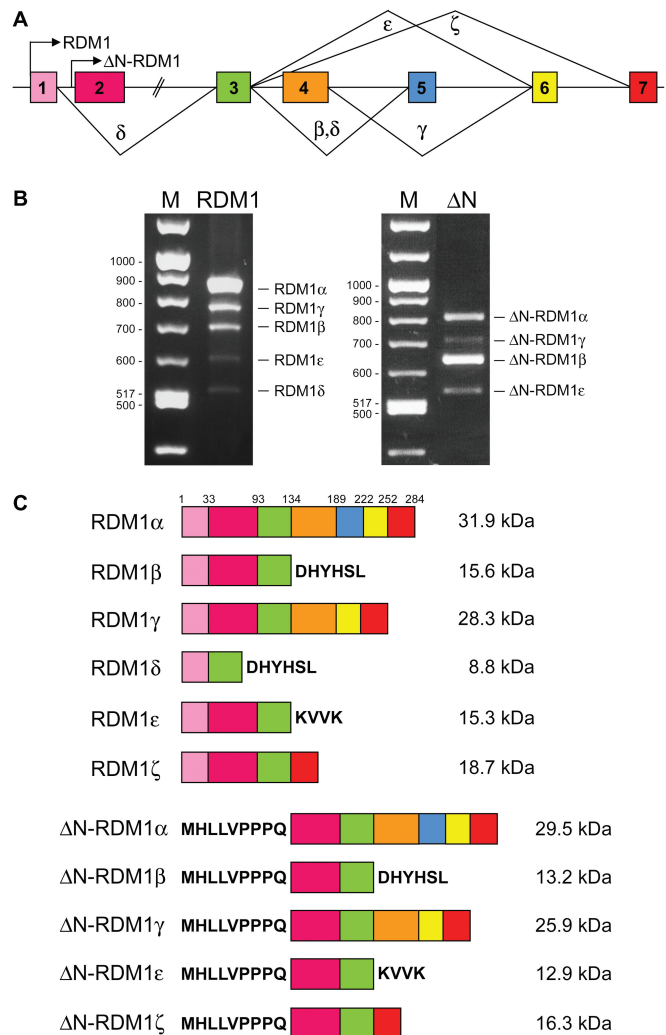


Figure 1. Structure of the human *RDM1* gene and the RDM1 protein isoforms. (A). Schema of the *RDM1* gene structure. Exons are numbered and arrows indicate the translation initiation codons used to produce proteins with long (RDM1) or short (Δ N-RDM1) N-terminal sequences. Greek symbols designate the splice variants detected in this study. Introns are not drawn to scale, and only the coding regions of exon 1 and 7 are shown. Whether the short and long N-terminal forms arise by use of two alternative transcription initiation sites within the *RDM1* gene is presently unknown. (B) RT-PCR analysis of the expression of the long (left panel) and short (right panel) N-terminal RDM1 isoforms in HEK293T cells. RT-PCR were carried out as described under 'Materials and Methods' section and analysed by agarose gel electrophoresis. (C). Structure of the RDM1 protein isoforms theoretically encoded by the *RDM1* cDNAs characterized in this study. Full-length RDM1 protein (284 aa) was renamed RDM1 α . Numbers refer to the first amino acid of each exon. See text for details.

In addition, the database suggested the existence of an alternative translation initiation codon located within intron 1 (position 495 on sequence accession number NC_000017.9) (Figure 1A). To learn more about the various forms of RDM1, we carried out a RT-PCR analysis on total RNA from HEK293T cells, using primer pairs designed to amplify isoforms containing the first ATG (hereafter referred to as long N-terminal forms). Gel analysis revealed a major band corresponding to the

expected *RDM1* product, as well as four smaller bands of lower intensity (Figure 1B, left panel). Similarly, reactions carried out with primers designed to amplify short N-terminal forms (containing the second ATG) revealed four bands (Figure 1B, right panel). Identical profiles were obtained with cDNA prepared from HeLa and MCF7 cells (data not shown, see also below). After sequencing, we established that the various bands obtained in each reaction corresponded to alternatively spliced variants. In total, nine *RDM1* cDNAs were characterized in this analysis. The structure of the *RDM1* proteins encoded by these cDNAs is illustrated in Figure 1C. Full-length *RDM1* was renamed *RDM1* α . We used the prefix Δ N- to designate isoforms translated from the second ATG, which lack exon 1 and contain an additional 9 aa in front of exon 2. Additional nomenclature was devised to reflect the presence of exons 2–7 (*RDM1* α and Δ N-*RDM1* α), or the exclusion of exon 4 (*RDM1* β and Δ N-*RDM1* β), exon 5 (*RDM1* γ and Δ N-*RDM1* γ), exons 2 + 4 (*RDM1* δ) and exons 4 + 5 (*RDM1* ϵ and Δ N-*RDM1* ϵ). Skipping of exon 4 in the β and δ isoforms results in a frame shift and premature termination within exon 5. Premature termination also occurs within exon 6 in the ϵ isoforms. In contrast, no frame shift accompanies the loss of exon 5 in the γ isoforms (Figure 1B). With the exception of *RDM1* δ , which does not contain exon 2, all isoforms contain exons 2 and 3. The RT-PCR data of Figure 1B suggest that *RDM1* α and Δ N-*RDM1* β are the most abundant forms produced from the first and second translation initiation codon, respectively. Finally, two additional isoforms (named *RDM1* ζ and Δ N-*RDM1* ζ , arising from the exclusion of exons 4–6) were identified in cells exposed to a mild heat shock (see below and Figure 1). Thus, alternative pre-mRNA splicing and differential usage of two translational start sites generate an extensive repertoire of *RDM1* isoforms.

Cytoplasmic and nuclear distribution of *RDM1* α

As a step to elucidating the function of the *RDM1* proteins, we first generated *RDM1* α fusion proteins containing N-terminal [enhanced green fluorescent protein (EGFP), Flag] or C-terminal [EGFP, mRFP, c-myc] tags and analysed their subcellular distribution in the human cell lines HEK293T and HeLa by transient transfection and confocal fluorescence microscopy. Images of representative cells are shown in Figure 2 and Supplementary Figure S1. In both cell types, and regardless of the nature and the location of the tag on *RDM1* α , the fusion proteins were found predominantly in the cytoplasm and, to a minor extent, in the nucleus. The fusion proteins were largely excluded from the nucleolus, which was identified by phase contrast illumination and chromatin staining (Figure 2A, B), and also by indirect immunofluorescence, using an antibody against the resident nucleolar protein nucleolin (Figure 2C). This pattern of distribution was also observed in HuH7 cells, as well as in living HEK293 cells and in cells stably expressing the EGFP-protein fusions (data not shown and see below). Treatment of the cells with leptomycin B (20 ng/ml), a known inhibitor of the nuclear exporter protein CRM1 (38,39), did not lead

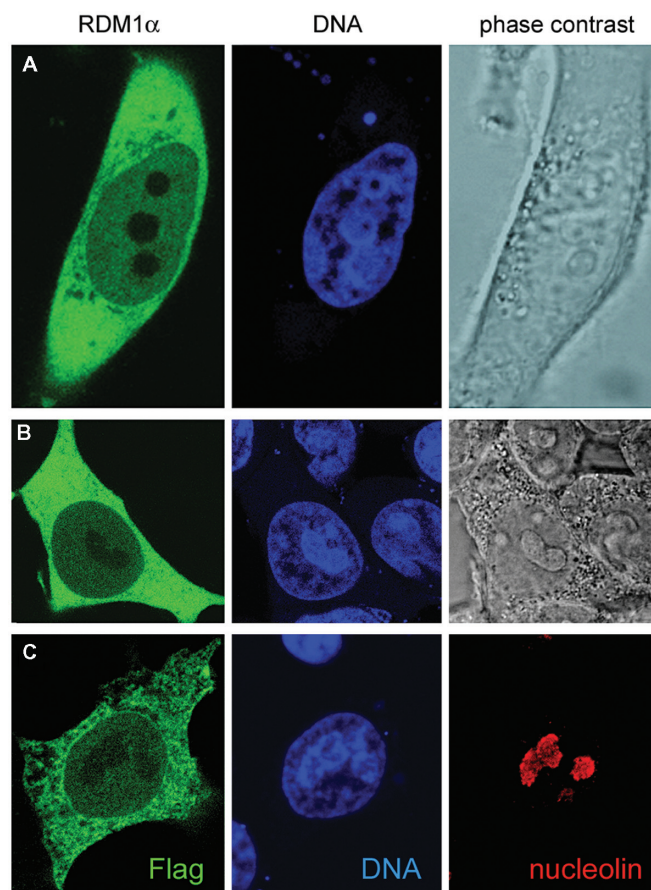


Figure 2. Subcellular localization of *RDM1* α . (A–B) Confocal microscopic images of HeLa cells expressing EGFP-*RDM1* α (A) and HEK293T cells expressing *RDM1* α -EGFP (B). Cells were fixed and counterstained with DRAQ5 (blue) prior to visualization. Green represents EGFP-tagged *RDM1* α . (C) HEK293T cells transfected with pFlag-*RDM1* α were double stained for nucleolin (red) and the Flag epitope (green). Cell transfection and immunofluorescence analysis were carried out as described under ‘Materials and methods’ section.

to the accumulation of the fusion proteins in the nucleus (data not shown), suggesting that *RDM1* α did not undergo CRM1-mediated nuclear-cytoplasmic shuttling.

Proteasome inhibition induces the subcellular redistribution of *RDM1* α and its nucleolar accumulation

We then tested whether various forms of cellular stress had any effect on *RDM1* α subcellular localization. Treatment with lactacystin or MG132, two specific proteasome inhibitors (40–42), resulted in a dramatic redistribution of the fusion proteins. As illustrated for EGFP-*RDM1* α in Figure 3A and B, the major effect of these drugs was the accumulation of the fusion proteins in the nucleolus. When the confocal settings were optimized for the visualization of the GFP signal in the nucleolus (Figure 3B, second image), or in cells expressing less protein fusions (Figure 3C), the fusion protein could be seen to form circular or more entangled structures that sometimes overlapped with peri-nucleolar chromatin (Figure 3C) or resided within the nucleolus (Figure 3B;

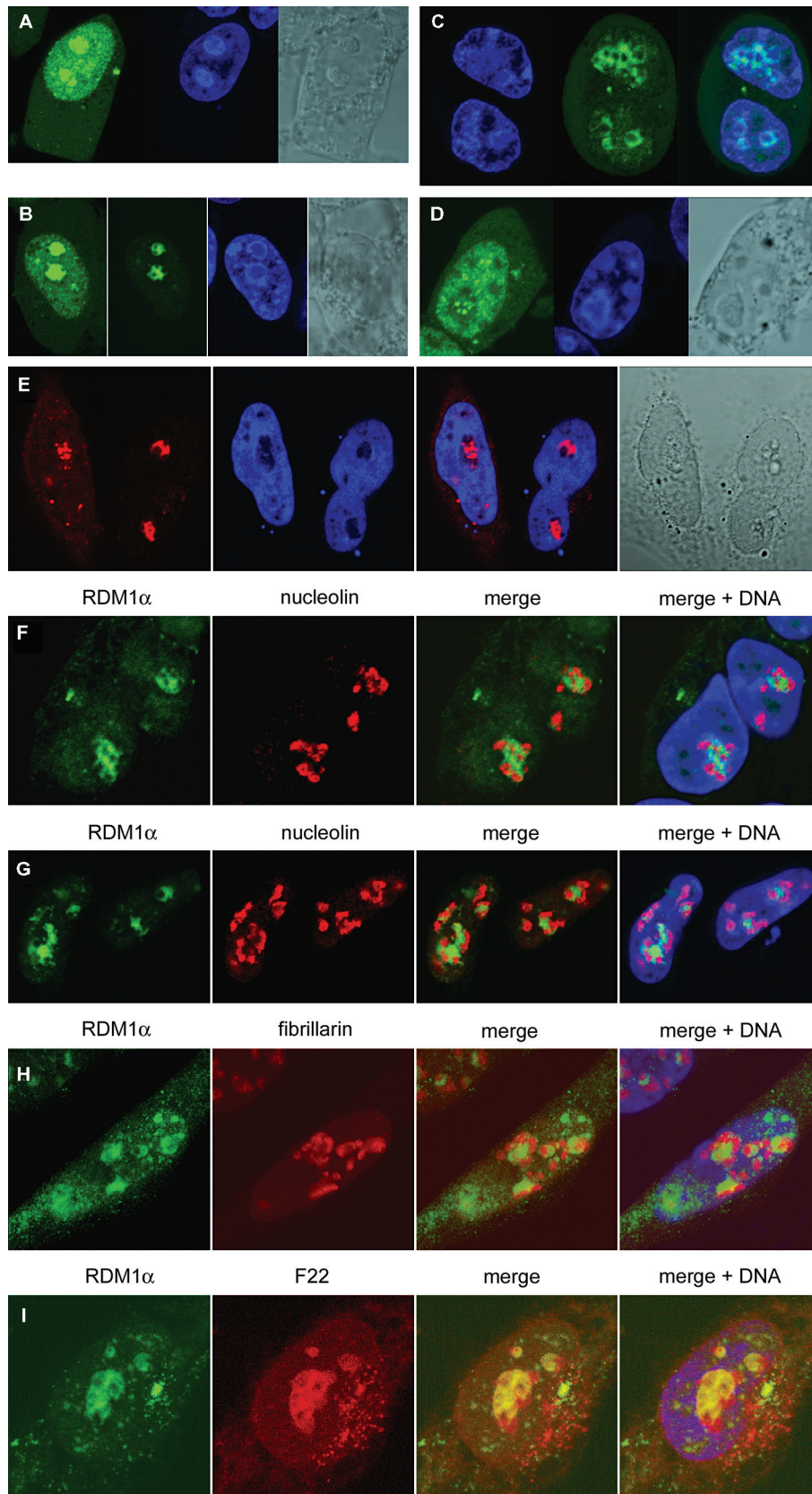


Figure 3. Subcellular redistribution and nucleolar accumulation of RDM1 α in response to proteotoxic treatment. (A–B) HEK293T cells transiently expressing EGFP-RDM1 α were treated with 10 μ M MG132 (A) or lactacystin (B) for 4 h, followed by fixation, counterstaining with DRAQ5 (blue) and confocal microscopic analysis. The second image of (B) is identical to the first, except that the confocal settings have been optimized for the

see also Figure 3E–G). In addition to these structures, accumulation of the green fluorescent protein (GFP) signal as nucleolar foci was also observed in some cells (Figure 3D). Identical results were obtained with cells expressing Flag-tagged RDM1 α (Figure 3E). Quantification of the subcellular distribution patterns of EGFP-RDM1 α in HeLa cells treated with MG132 (10 μ M) indicated that after 2 and 8 h of treatment, nucleolar accumulation of the fusion protein as circular/entangled structures could be observed in about 40% (138 cells examined) and 74% (73 cells examined) of the cells, respectively. At these time points, the percentages of cells displaying general accumulation of the GFP signal in the nucleus without detectable nucleolar accumulation were 53 and 16%, respectively, and <10% of the cells showed nucleolar foci.

To learn more about the localization of RDM1 α within the nucleolus, cells expressing RDM1 α -EGFP were treated with lactacystin or MG132 and stained with an antibody to nucleolin, a very abundant nucleolar protein involved in ribosomal DNA (rDNA) transcription, rRNA processing and ribosome assembly (43). As illustrated in Figure 3F and G, although RDM1 α and nucleolin were very closely associated, little or no overlap was observed between the two proteins. Likewise, RDM1 α did not co-localize with fibrillarin, a factor involved in pre-rRNA processing (44,45) (Figure 3H). However, RNA staining with the RNA-selective dye F22 (37) revealed an extensive overlap between RDM1 α and nucleolar RNA, even though large regions of the nucleolar RNA did not contain RDM1 α (Figure 3I). Inhibition of the proteasome has been shown to induce the disruption of nucleolar architecture and alter the distribution of nucleolar proteins, including nucleolin and fibrillarin, as well as rRNA and rRNA precursors (46). Thus, partial segregation of rRNA precursors and their processing factors was observed in response to proteasomal inhibition, and factors involved in early and late preRNA processing, which overlapped extensively in the absence of stress, underwent spatial separation after MG132 treatment (46). Our observations therefore suggest that part of the rRNAs redistributed in response to proteasomal inhibition might become targets for RDM1 α accumulating in the nucleolus.

In addition to promoting its nucleolar accumulation, proteotoxic treatment also affected the overall distribution of RDM1 α in the nucleoplasm. In particular, dot-like or more irregular subnuclear structures containing RDM1 α were found to accumulate in many cells treated with MG132 or lactacystin (see for instance, Figure 3A,

B and D). We considered the possibility that these structures corresponded to specific nuclear bodies. When stressed cells were stained with antibodies directed against the promyelocytic leukemia (PML) protein, a component of PML bodies (47), extensive juxtaposition or colocalization of some RDM1 α -containing structures with PML was observed (Figure 4A), suggesting the association of RDM1 α with PML bodies. These nuclear bodies have been implicated in several processes such as sensing of cellular stress (48), transcriptional regulation (49,50) and chromatin remodeling (51). Several indications also suggest that they function as storage sites, to regulate protein activity within the nucleus (47). In many cells, PML-positive foci also accumulated in the nucleoli of cells treated with proteasomal inhibitors (Figure 4B), consistent with published studies showing that a fraction of PML protein dissociated from the PML bodies to relocate to the nucleolus in response to MG132 treatment (52). However, we found no correlation between the presence of PML in the nucleolus and that of RDM1 α (data not shown; see also Figure 4A, where no PML protein is found in the nucleoli colonized by RDM1 α). Similar observations were made with cells treated with lactacystin (data not shown).

Some RDM1 α foci were also found to colocalize with, or be adjacent to Cajal nuclear bodies (CBs), identified by the marker protein p80 coilin (Figure 4C). CBs play a role in the transport and maturation of small nuclear ribonucleoproteins (snRNPs) involved in pre-mRNA processing, as well as small nucleolar RNPs (snoRNPs) involved in rRNA modification and processing; they have also been implicated in the cell response to stress (53). In addition, whereas CBs do not colocalize with PML bodies, they are often found in close proximity, suggesting the exchange of components (47,53). The fact that RDM1 α can be found in association with both types of nuclear bodies may therefore suggest some concerted action of PML bodies and CBs during proteotoxic stress. Under normal conditions, cells displaying nuclear RDM1 α foci were infrequent. However, colocalization with PML bodies or CBs could sometimes be observed in foci-positive cells (Figure 4D and E). Taken together, these observations suggest that RDM1 α interacts with PML bodies and CBs under normal conditions, and that this association greatly increases in response to proteotoxic stress. Whether the recruitment of RDM1 α to PML and CBs serves as a sequestration mechanism to regulate its activity, or reflects a biochemical function within these bodies, is currently unknown.

analysis of the GFP signal within the nucleolus. (C) HEK293 cells stably expressing RDM1 α -EGFP were treated with 10 μ M lactacystin for 8 h and living cells were analysed following counterstaining with DRAQ5. (D) HEK293T cell displaying the accumulation of the EGFP-RDM1 α protein as nucleolar foci in response to treatment with MG132 (10 μ M, 4 h). (E) HeLa cells expressing Flag-RDM1 α were treated with 10 μ M MG132 for 4 h, followed by fixation and staining of the Flag epitope (red). Nucleolar foci and entangled structures can be seen in the left and right cells shown on this image, respectively. (F–H) Lack of colocalization of stress-induced, nucleolar RDM1 α with nucleolin and fibrillarin. (F) HEK293T cells expressing RDM1 α -EGFP were treated with 10 μ M lactacystin for 8 h, followed by fixation and staining for nucleolin. Nuclei were counterstained with DRAQ5 (blue). (G) HEK293 cells stably expressing RDM1 α -EGFP were treated with 25 μ M MG132 for 8 h and analysed as described for (F). (H) HeLa cells expressing RDM1 α -EGFP and Fibrillarin-RFPCherry were treated with 10 μ M MG132 for 8 h followed by fixation, counterstaining with DAPI (blue) and visualization. Signals from EGFP (green) and nucleolin or fibrillarin (red) were merged, revealing distinct distribution patterns. (I) Colocalization of RDM1 α with nucleolar RNA in MG132-treated cells. HeLa cells expressing RDM1 α -EGFP were treated with MG132 (10 μ M MG132, 8 h) and the RNA was visualized with the cell-permeant, RNA-specific dye F22, followed by processing as for (H). In the merged image, RDM1 α -EGFP (green) and RNA (red) coincide extensively (yellow) within the nucleoli.

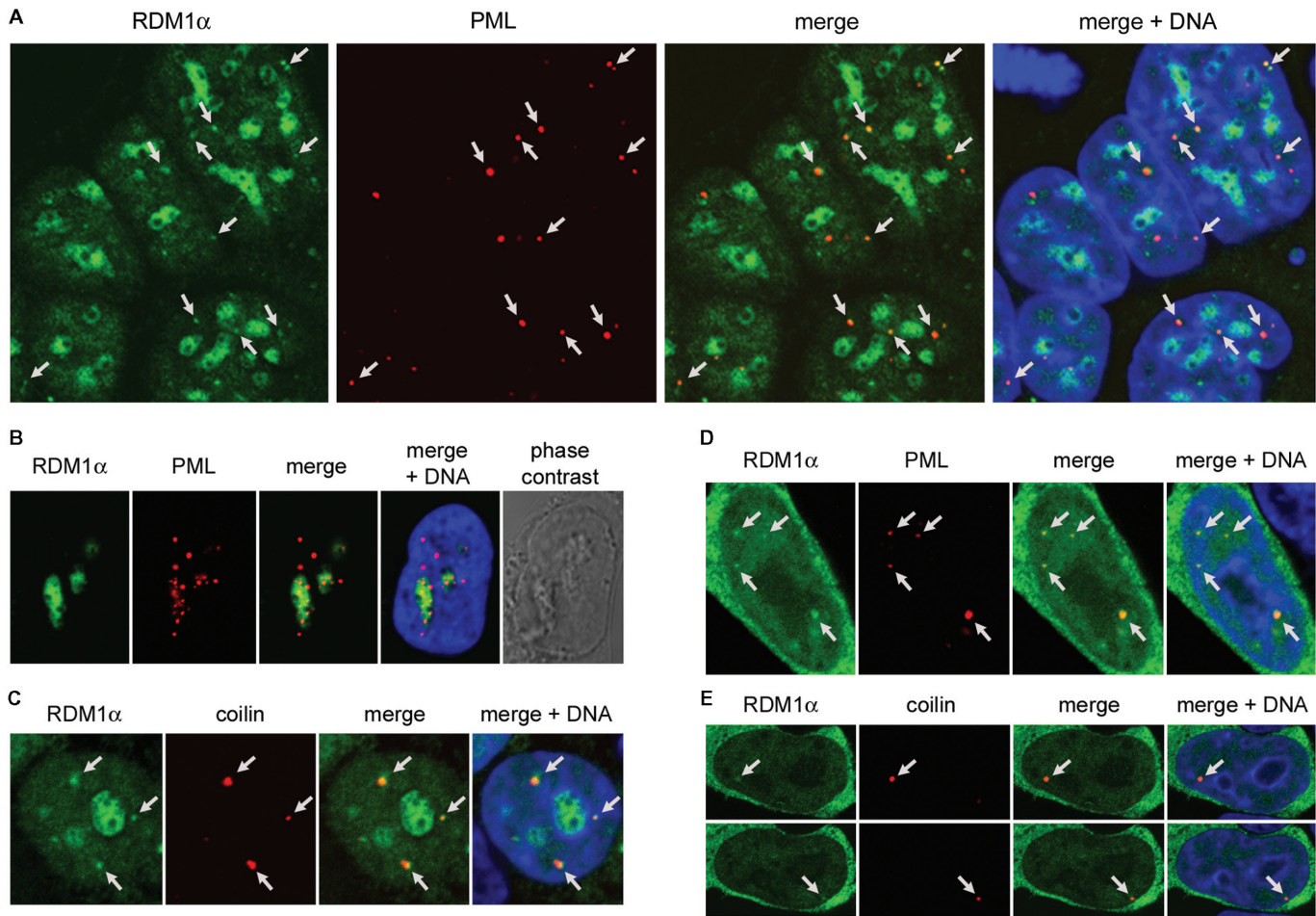


Figure 4. Association of RDM1 α -EGFP with PML and CBs. (A) Confocal micrographs of RDM1 α -EGFP-transfected HEK293T cells following treatment with MG132 (10 μ M, 4 h) and staining of PML (red). The DNA was counterstained with DRAQ5 (blue). In addition to accumulating in the nucleoli, RDM1 α can be seen in numerous dot-like nuclear structures. Several of these dots (some of which are indicated by arrows) coincide with or are in close proximity to PML bodies as illustrated in the merged image. Note that, in the cells depicted here, no PML protein is detected in the nucleoli colonized by RDM1 α . (B) Image of a MG132-treated cell (10 μ M, 8 h) showing the partial accumulation of PML protein in nucleoli colonized by RDM1 α . (C) HEK293T cells transfected with RDM1 α -EGFP were treated with MG132 (10 μ M, 2 h), followed by staining of the CB marker coilin (red). As illustrated in the merged image, some of the dot-like structures containing RDM1 α (indicated by arrows) colocalize, or are in close contact with CBs in MG132-treated cells. (D–E) Association of RDM1 α with PML bodies (D) and CBs (E) in unstressed cells. The panels in (E) represent two sections of the same cell showing dot-like structures containing RDM1 α (indicated by arrows) that colocalize with CBs.

Mild heat stress induces accumulation of RDM1 α in the nucleolus

Inhibition of proteasome-mediated protein degradation leads to the accumulation of proteins normally targeted for degradation as part of the execution of certain cellular programmes or because they are aggregated, misfolded or damaged (41). Accumulation of denatured proteins can also be triggered by conditions such as heat shock (54). Therefore, we determined whether a heat-shock stress altered RDM1 α subcellular distribution in HEK293T and HeLa cells. Following transfection with plasmids expressing the RDM1 α protein tagged with EGFP, the cells were subjected to a mild heat-shock treatment (43°C, 30 min) before fixation and analysis. As illustrated representatively for HEK293T cells in Supplementary Figure S2A, the fusion protein accumulated in the nucleolus in response to heat shock, forming circular and more entangled structures. This accumulation,

which affected essentially all cells, was reversible, as more than 90% of the cells displayed normal subcellular distribution of the fusion proteins after a recovery period of 2 h at 37°C (data not shown). Furthermore, incubation of the cells with cycloheximide (20 μ g/ml) for 1 h prior to heat shock did not inhibit the nucleolar accumulation of RDM1 α (Supplementary Figure S2B), indicating that the heat-shock induced relocalization of RDM1 α did not depend on protein neo-synthesis.

Subcellular distribution of RDM1 α during transcriptional arrest

Transcriptional inhibition represents a form of stress that greatly affects the architecture of the nucleolus. Transcriptional arrest mediated by inhibition of RNA polymerase I and/or II elicits nucleolar segregation and the formation of nucleolar caps consisting of nucleolar components originating from the original nucleolus,

as well as nuclear components (55–57). A comprehensive study using concentrations of actinomycin D sufficient to inhibit both RNA pol I and II (resulting in fully segregated nucleoli), has shown that nucleolar segregation is a dynamic process that also involves the redistribution of nucleoplasmic proteins and RNAs (34). Thus, in response to transcriptional arrest, the defining regions of the nucleolus [fibrillar centres, dense fibrillar components and granular components (GC)] redistributed in domains called nucleolar caps and central body (that was originally the GC). Although some nucleolar proteins (mainly from the GC) dispersed in the nucleoplasm after transcriptional arrest, these domains retained many of their original proteins and RNAs. In addition, proteins and RNA components from many nuclear bodies relocated to discrete nuclear caps, whereas numerous nucleoplasmic proteins, including several RNA-binding proteins, formed large nucleolar caps (34, and references therein). Because it can occur under physiological states and can be followed by nucleolar reassembly, Shav-Tal *et al.* (34) have proposed that nucleolar segregation evolved as a flexible mechanism to redistribute specific nuclear components in response to transcriptional arrest, whilst keeping certain basic interactions, thus facilitating efficient reassembly upon transcriptional resumption.

To determine its possible involvement in nucleolar capping caused by transcriptional arrest, we examined the subcellular distribution of RDM1 α in response to specific inhibition of RNA pol I (50 ng/ml actinomycin D, 2 h) (33), inhibition of both RNA pol I and pol II (5 μ g/ml actinomycin D, 2 h) (34) or specific inhibition of RNA pol II (50 μ g/ml α -amanitin, 5 h) (35). In all cases, RDM1 α remained predominantly cytoplasmic, whilst being also present in the nucleus, as observed with untreated cells (Supplementary Figure S3). This suggested that ongoing transcription was not required for its nucleocytoplasmic distribution. In the majority of cells, low levels of actinomycin D, which caused p80 coilin to redistribute at the nucleolar periphery, had little apparent effect on the subcellular localization of RDM1 α (data not shown). In a few cells, however, some RDM1 α protein could be seen at the rim of the nucleolus, where it partially overlapped with p80 coilin, as well as in the centre of the nucleolus (Supplementary Figure S3A). In contrast, cells treated with high levels of actinomycin D, consistently showed the relocalization of a fraction of RDM1 α in nucleolar rings or cap-like structures that were surrounded by a dense chromatin ring from which the protein was excluded, and some protein also colonized the centre of the nucleolus (Supplementary Figure S3B). Little or no overlap was observed between RDM1 α and p80 coilin in these structures. Nucleolar relocalization of RDM1 α was much less apparent when α -amanitin was used to inhibit RNA pol II specifically, although in some instances a fraction of RDM1 α could also be seen at the nucleolar periphery (Supplementary Figure S3C).

Because *RDM1* null cells display increased sensitivity to cisplatin (27), and since cisplatin has been shown to inhibit rRNA synthesis and cause nucleolar segregation (58), we tested whether RDM1 α relocated to nucleolar caps in response to cisplatin. However, no redistribution

of RDM1 α was seen following treatments with doses of cisplatin at which nucleolar segregation is reported to occur [10 μ g/ml, 8 h (58)] (data not shown). Taken together, our observations suggest that efficient nucleolar capping by RDM1 α requires the extensive nucleolar segregation that occurs upon inhibition of both RNA pol I and pol II (34, and references therein).

Heat-shock sensitivity of *RDM1*-deficient chicken DT40 cells

We next wanted to examine the importance of the *RDM1* gene in the cellular response to proteotoxic stress and heat shock. We have previously described the construction of null cells lacking *RDM1* by gene disruption in the chicken B-lymphoid cell line DT40 (27). We first compared the survival of wt and *RDM1*^{-/-} cells following exposure at various temperatures for different periods. DT40 cells grow at the maximal rate at the physiological temperature of 39.5°C, and their survival at high temperatures depends on conserved as well as avian-specific heat-shock transcription factors (59). No differences in viability were observed at the moderately high temperature of 42°C (data not shown). However, *RDM1*^{-/-} cells displayed a mild increase in sensitivity to a heat shock carried out at 45°C (Figure 5A). Finally, compared to wt cells, *RDM1*^{-/-} cells were not hypersensitive to MG132 (Figure 5B).

Transcripts encoding novel isoforms of human RDM1 accumulate in response to heat shock

We next used semi-quantitative RT-PCR to examine the mRNA expression patterns of the RDM1 isoforms in HEK293T, HeLa and MCF7 cells subjected to a heat shock (43°C, 45 min). As representatively illustrated for HEK293T cells in Figure 6A, the expression pattern of the long N-terminal forms was essentially unchanged following heat shock, except for a slight increase in the intensity of the band corresponding to RDM1 ϵ , and the apparent accumulation of RDM1 δ . However, after sequencing, we established that the observed accumulation was due to the presence of a novel isoform with the same size as RDM1 δ . This splice variant, which lacks exons 4–6, was named RDM1 ζ (see Figure 1). We confirmed the heat-shock inducibility of RDM1 ζ expression using specific PCR primers (Figure 6B). Likewise, the expression pattern of the short N-terminal forms revealed that a novel form corresponding to Δ N-RDM1 ζ accumulated in a heat-shock dependent manner, whereas the other Δ N-isoforms were downregulated in response to heat shock (representatively illustrated for MCF7 cells in Figure 6C). Taken together, these data suggest that the expression of the human *RDM1* gene is modulated by heat-shock stress.

Nuclear and nucleolar localization determinants in exon 3 of RDM1

Because RDM1 α is present both in the cytoplasm and nucleus and can also relocate to the nucleolus, we next sought to identify the determinants of its subcellular distribution. Since exon 3 is common to all the isoforms reported here, we first looked whether it contained specific

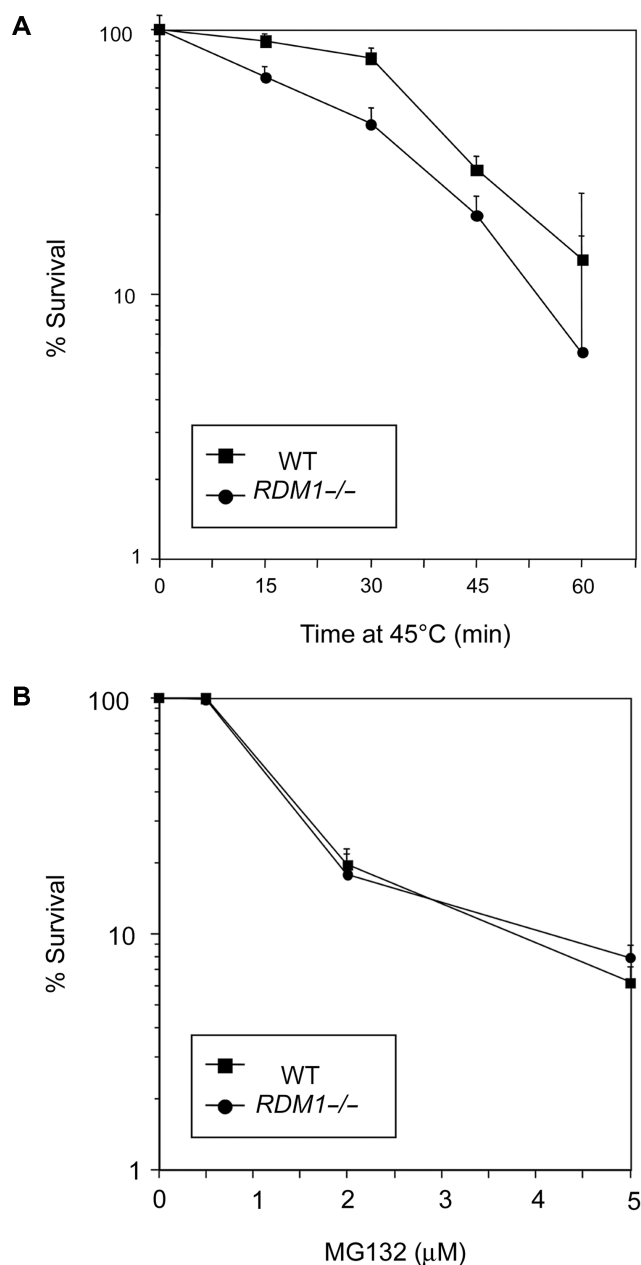


Figure 5. Heat-shock sensitivity of *RDM1* null chicken DT40 cells. (A) Wt and homozygous *RDM1*-deficient (*RDM1*^{-/-}) cells grown at 39.5°C were incubated at 45°C for the indicated periods, and surviving cells were counted by colony formation assays. (B) *RDM1* null cells are not hypersensitive to MG132. Wt and *RDM1*^{-/-} cells were treated with the indicated concentrations of MG132 for 24h, followed by staining with PI and FACS analysis. Survival is expressed as a percentage, using untreated cells as the 100% value. Colony survival assays and FACS analysis were carried out as described under 'Materials and Methods'. Experiments were done in triplicates, and the results are shown with standard deviations.

intracellular localization signals by expressing a EGFP-RDM1₉₀₋₁₃₃ fusion protein in HeLa cells. (A schematic of all the constructs used in this study is shown in Figure 9F). As illustrated in Figure 7A, the fusion protein displayed a prominent signal in the nucleus, and in particular in the nucleolus; only little GFP signal was detected in the cytoplasm where a punctuate pattern was sometimes

observed. Exon 3 must therefore contain nuclear and nucleolar localization domains. Classical nuclear localization signals (NLS) consist of one (monopartite NLS) or two (bipartite NLS) stretches of basic amino acids residues (60). Likewise, stretches of basic residues (in single or multiple copies) have been found in the nucleolar localization signal (NoLS) of numerous proteins (25,61, and references therein), whereas other proteins rely on their nucleic acid-binding domains to associate with the nucleolus (62). The 41-aa sequence of exon 3 contains a stretch of basic residues at position 98–100 (RHK), as well as the previously identified RD motif (aa 104–132), which the evidence suggests is involved in modulating the DNA-binding properties of RDM1 (28) (Figure 7D). The RD motif contains several aromatic residues that might be involved in nucleic acid interactions. In a preliminary experiment, we found that the RD motif on its own was unable to mediate the nucleolar recruitment of EGFP (data not shown). As a step to further delineate the nuclear/nucleolar targeting regions of RDM1, we therefore substituted AAA for either RHK at position 98–100, or YYF at position 120–122 of exon 3, within the EGFP-RDM1₉₀₋₁₃₃ fusion protein. The (120–122) YYF-AAA mutation did not affect the subcellular distribution of the fusion protein, which was still essentially nuclear and nucleolar (Figure 7B). However, compared to wt exon 3, a brighter GFP signal was consistently observed in the nucleolus of cells expressing the (120–122) YYF-AAA variant, suggesting that the mutation affected intranuclear trafficking. In contrast, the (98–100, RHK-AAA) mutation dramatically reduced the levels of GFP signal observed in the nucleolus (Figure 7C), indicating that this stretch of residues was a crucial component of the NoLS in exon 3. In addition, the (98–100, RHK-AAA) variant accumulated less predominantly in the nucleus, and a more intense GFP signal was found instead in the cytoplasm, suggesting that aa 98–100 also played a role in the transport of exon 3 into the nucleus. Identical observations were made with HEK293T cells (data not shown).

The localization data obtained with EGFP-RDM1₉₀₋₂₈₄ suggests that exon 3 might be involved in the stress-induced nucleolar accumulation of RDM1 α . To test this notion, we analysed the subcellular distribution of an EGFP-RDM1 α - Δ E3 fusion lacking exon3, under normal conditions or following a mild heat stress. In the absence of any stress, we found that the fusion protein was cytoplasmic and nuclear, but excluded from the nucleolus (Figure 7E). However, it still accumulated in the nucleolus in response to heat shock (Figure 7F). Nucleolar accumulation of the EGFP-RDM1 α - Δ E3 fusion was also observed after treatment with proteasome inhibitors (data not shown, see also below). These experiments suggest that other domains of RDM1 α can mediate its nucleolar targeting.

Subcellular distribution of the RRM domain of RDM1

RRM domains have been shown to mediate the intracellular localization of numerous proteins. The RRM identified by Pfam spans residues 17–92 of RDM1;

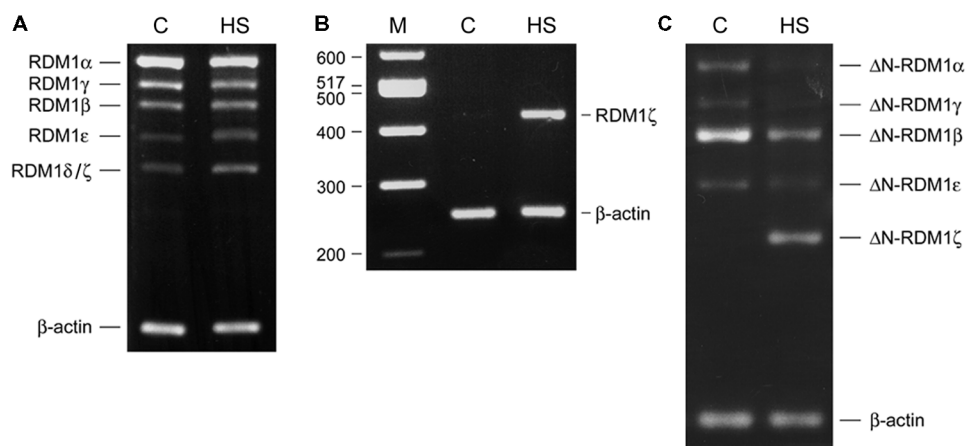


Figure 6. Effect of mild heat-shock stress on human *RDM1* gene expression. (A) Semiquantitative analysis of the cDNA expression pattern of the long N-terminal *RDM1* isoforms in control and heat-shocked HEK293T cells. (B) Heat-shock inducible upregulation of *RDM1* ζ . Specific PCR amplification was carried out using the primer pair EV041 (containing the ATG) and EV305 (which overlaps the junction between exon 3 and 7) to produce a diagnostic band of 422 n. (C) cDNA expression pattern of the short N-terminal *RDM1* isoforms in control and heat-shocked MCF7 cells, illustrating the downregulation of Δ N-*RDM1* α , - β , - γ , and - ϵ , and the upregulation of Δ N-*RDM1* ζ in response to heat shock. RNA isolation and semiquantitative RT-PCR analyses were carried out as described under 'Materials and Methods'. Primers EV041 and EV042 (long N-terminal isoforms), EV254 and EV042 (short N-terminal isoforms) were used in the reactions, together with primers for β -actin as internal control (see Supplementary Table 1). C, control; HS, heat shock; M, molecular weight markers. See text for details.

it initiates within exon 1 (aa 1–32), which contains its putative RNP2 signature (LLVWEL) (aa 17–22), and terminates at the end of exon 2 (aa 33–92). We therefore examined the subcellular distribution of an EGFP-*RDM1*_{1–92} fusion protein. Figure 8A (left panel) shows that the fusion protein is localized primarily in the nucleus, with little GFP signal in the cytoplasm. This indicates that, like exon 3, the RRM of *RDM1* can also mediate nuclear localization of EGFP. Whereas the EGFP-*RDM1*_{1–92} fusion is clearly also nucleolar, it is mainly in the nucleoplasm, in contrast to what was observed with the EGFP-exon3 fusion. However, nucleolar accumulation of the EGFP-*RDM1*_{1–92} fusion was observed in response to heat shock (Figure 8A, right panel).

To further explore the possible redundancy played by its RRM and exon 3 in the subcellular localization of *RDM1* α , we next examined the distribution of deletion constructs lacking exons 1–2 (EGFP-*RDM1*_{90–284}) or exons 1–3 (EGFP-*RDM1*_{133–284}). In the absence of stress, both fusion proteins showed a subcellular distribution reminiscent of *RDM1* α , being predominantly cytoplasmic and also nuclear but not nucleolar (Figure 8B and C, left panels). Moreover, both displayed nucleolar accumulation in response to heat shock (Figure 8B and C, right panels) or proteasomal inhibition (Supplementary Figure S4). Taken together, these observations suggest that the C-terminal half of *RDM1* α (exons 4–7) contains cytoplasmic retention domains as well as determinants involved in its stress-induced nucleolar accumulation.

Because *RDM1* α colocalized extensively with nucleolar RNA in cells treated with inhibitors of the proteasome, and to explore the role of its proposed nucleic-acid binding motifs in mediating this interaction, we next studied the distribution of the EGFP-*RDM1*_{90–284} and EGFP-*RDM1*_{133–284} fusions relative to nucleolin and RNA in HEK293T cells treated with MG132. In both

cases, little or no overlap was seen between the fusion proteins and nucleolin. In addition, the GFP signal of the fusion proteins still coincided extensively with nucleolar RNA (Supplementary Figure S4A and B). Similar observations were made with the EGFP-*RDM1* α - Δ E3 construct (data not shown). These observations suggest that *RDM1* α may be recruited to nucleolar RNA indirectly, via interactions with protein partners. Similarly, the loss of exons 1–3 did not prevent the association of the fusion proteins with PML or p80 coilin (data not shown), indicating that the ability of *RDM1* α to interact with nucleic acids is not required for its recruitment to PML and CBs.

Subcellular distribution of other *RDM1* isoforms

The isoforms reported in this study arise from alternative splicing events involving only splice donor and acceptor sequences that delineate the exons of the full-length *RDM1* α protein (Figure 1A). Therefore, in addition to providing insights into their localization and function, the study of these isoforms should also be indicative of the contribution of its various exons to the subcellular location of *RDM1* α . Figure 9 illustrates the subcellular distribution patterns of selected isoforms expressed as EGFP-protein fusions and observed in the absence of stress (left panels) or in response to heat shock (right panels). In this report, we restricted our analysis to the long N-terminal isoforms. We found that *RDM1* β , which lacks exons 4–7, was primarily nuclear and nucleolar (Figure 9A), consistent with the localization determinants assigned to the RRM and exon 3. In addition, the nucleolar distribution pattern of *RDM1* β was heterogeneous, some transfectants displaying more GFP signal in the nucleolus than others (Figure 9A, upper and lower panels). A predominantly nuclear and nucleolar distribution was also observed with the heat-shock inducible

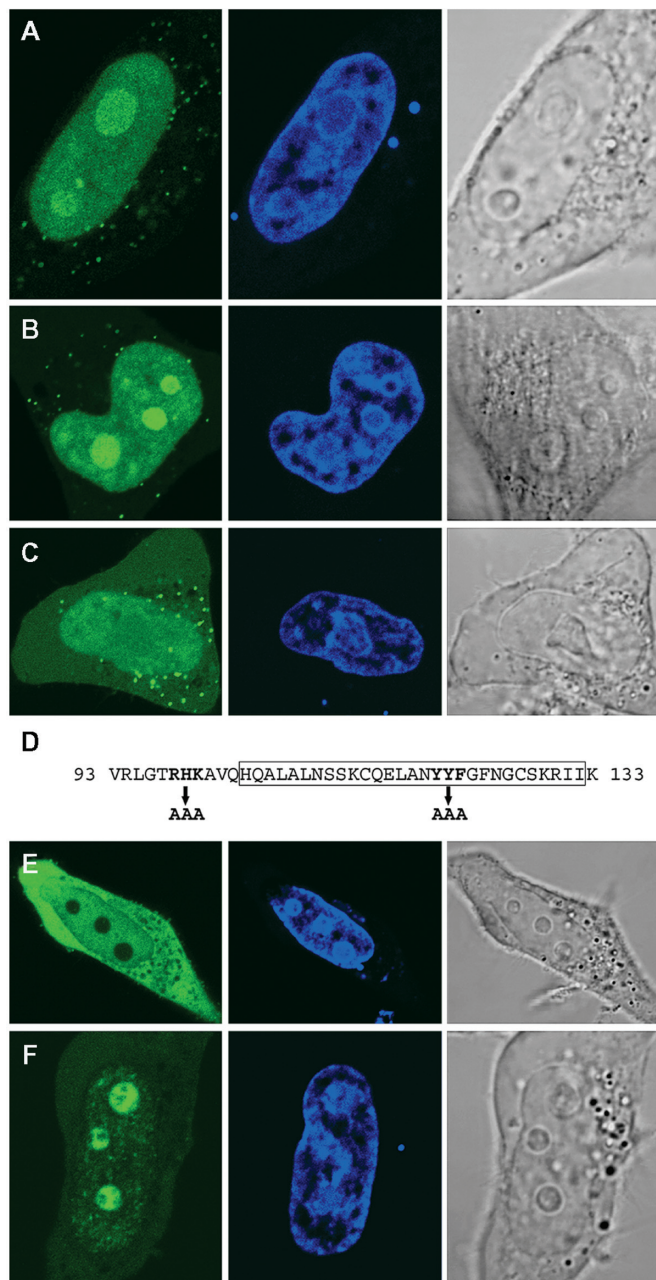


Figure 7. Nuclear and nucleolar localization signals in exon 3 of RDM1 α . (A–C) HeLa cells expressing either wt exon 3 (A), the (120–122) YYF-AAA variant (B) or the (98–100) RHK-AAA variant (C) as EGFP-RDM1_{90–133} fusion proteins were fixed and observed by direct fluorescence, under a confocal microscope. (D) Amino-acid sequence of human RDM1 exon 3, showing the position of the mutations carried out as well as the RD motif (boxed). (E–F) Deletion of exon 3 does not prevent the nucleolar accumulation of RDM1 α in response to heat stress. HeLa cells expressing EGFP-RDM1 α - Δ E3 were observed in the absence of stress (E) or following mild heat-shock treatment (43°C, 30 min) (F). Green represents EGFP-tagged exon 3 or RDM1 α - Δ E3 and blue represents DRAQ5-stained nuclei. See text for details.

isoform RDM1 ζ (Figure 9B). Importantly, RDM1 γ , which only lacks exon 5, was also located predominantly in the nucleus; little GFP signal was observed in the cytoplasm. (Figure 9C). However, RDM1 γ was still essentially non-nucleolar. Taken together, these

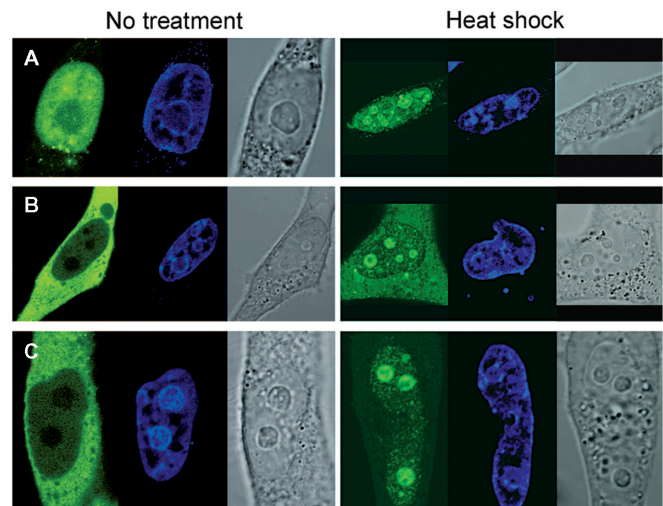


Figure 8. Subcellular localization of the RRM domain as well as N-terminal truncation mutants of RDM1 α . Confocal microscopic visualization of control (left panel) or heat-shocked (right panel) HeLa cells expressing EGFP-RDM1_{1–92} (A), EGFP-RDM1_{90–284} (B) or EGFP-RDM1_{133–284} (C). Cells were fixed and counterstained with DRAQ5 (blue) prior to visualization.

observations suggest that the nuclear/nucleolar targeting domains present in the N-terminal part of RDM1 α (exons 1–3) must be controlled in part by a cytoplasmic retention signal located in exon 5, as well as by other domains that modulate intranuclear trafficking and nucleolar accumulation of the RDM1 proteins. These notions were, however, complicated by the analysis of the RDM1 δ isoform (consisting solely of exons 1 and 3), which was found evenly distributed in the cytoplasm and the nucleus despite lacking exons 4–7 (Figure 9D). This pattern contrasted with the almost exclusive nuclear localization of exon 3 (see Figure 7A), indicating that, in the absence of stress, the nuclear/nucleolar targeting functions mediated by exon 3 can be partially neutralized by sequences located in exon 1. Finally, all the isoforms studied here displayed nucleolar accumulation in response to heat shock (right panels of Figure 9A–D) or proteotoxic treatment (data not shown).

We next analysed the effect of actinomycin D on the subcellular distribution of RDM1 β and RDM1 γ , which are predominantly nuclear under normal conditions but differ by their degree of nucleolar occupancy. RDM1 β (which is present in the nucleolus in the absence of stress) was still distributed throughout the nucleus in cells treated with actinomycin D (5 μ g/ml, 2 h), with the exception of those regions that stained strongly for DNA. However, a bright GFP signal was now concentrated in concave nucleolar caps (Figure 9E, panel a). The type(s) of nucleolar cap in which RDM1 β resides following inhibition of transcription is currently unknown. RDM1 γ which, like RDM1 α , is essentially excluded from the nucleolus in the absence of stress, did not strongly relocate in nucleolar caps during transcriptional arrest. Instead, a fraction of it assembled into nucleolar cap- and ring-like structures encircled by a dense chromatin ring, reminiscent

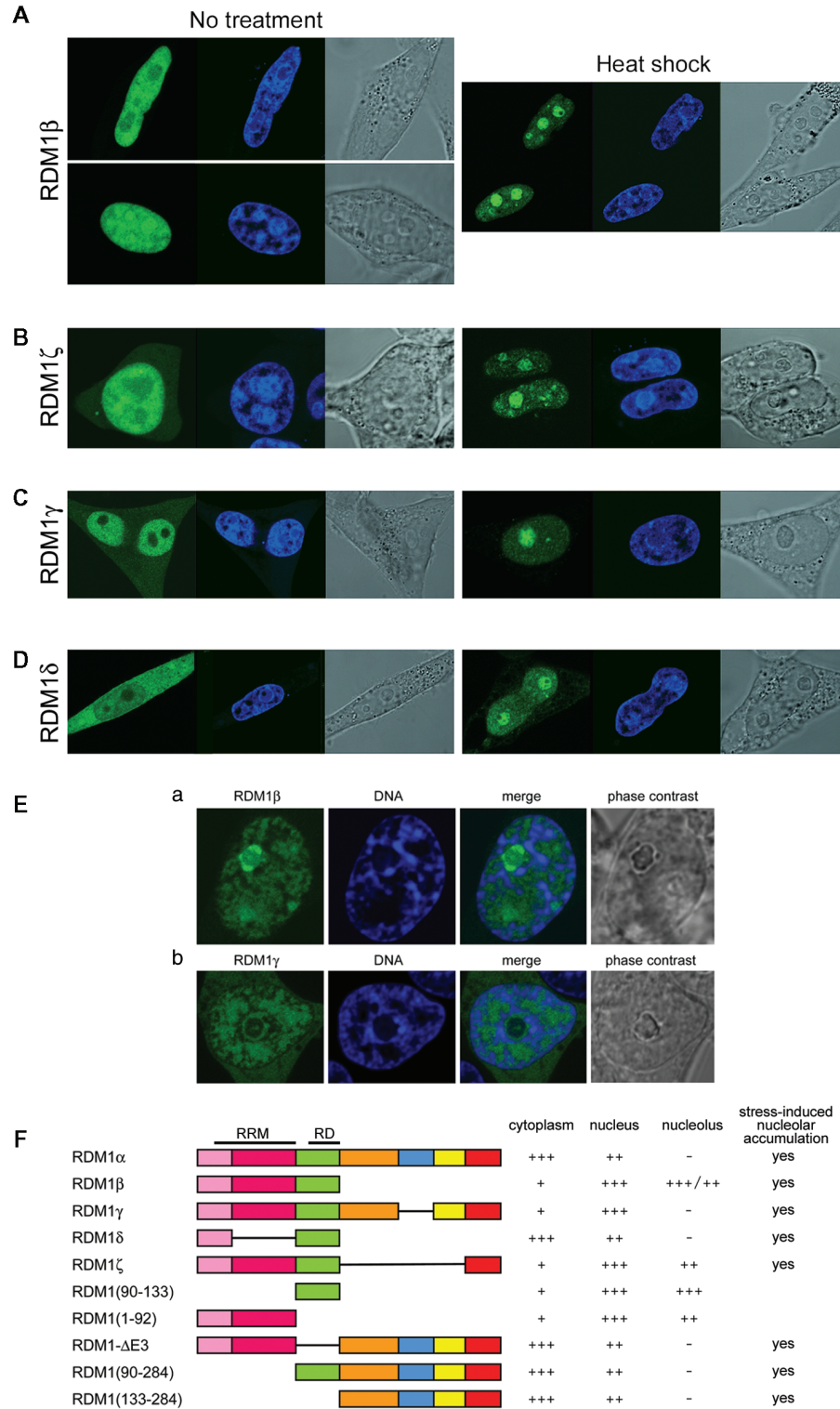


Figure 9. Subcellular distribution of various long N-terminal RDM1 isoforms. (A–D) HeLa or HEK293T cells expressing the cloned cDNAs as EGFP-RDM1 fusions were left untreated (left panels) or treated with a mild heat shock (right panels) prior to fixation and direct fluorescence analysis. (A) RDM1 β in HeLa cells. The upper and lower panels illustrate the differences in the levels of nucleolar GFP signal observed among transfectants. (B) RDM1 ζ in HEK293T cells. (C) RDM1 γ in HeLa cells. (D) RDM1 δ in HeLa cells. Green represents the EGFP-tagged proteins and blue represents DRAQ5-stained nuclei. (E) Effect of high levels of actinomycin D on the association of RDM1 β and RDM1 γ proteins with nucleolar caps. HEK293T cells transfected with EGFP-RDM1 β (panel a) or EGFP-RDM1 γ (panel b) were treated with actinomycin D (5 μ g/ml) for 2 h, followed by fixation, DNA counterstaining with DRAQ5 and confocal microscopy. Strong accumulation of RDM1 β is seen in nucleolar caps, whereas the distribution pattern of RDM1 γ is more reminiscent of that observed with RDM1 α . (F) Schematic representation of the RDM1 isoforms and deletion constructs examined in this study and summary of their subcellular distribution. The position of the RRM and RD motifs is indicated above the structure of RDM1 α .

of those seen with RDM1 α (Figure 9E, panel b). Because RDM1 β consists only of exons 1–3, our observations suggest that the remaining C-terminal exons of RDM1 α and RDM1 γ play a role in retaining these isoforms in the nucleoplasm, thereby preventing a strong association with components of the nucleolar caps during transcriptional arrest.

In summary, in the absence of stress, the long N-terminal isoforms of RDM1 showed subcellular distribution patterns ranging from predominantly cytoplasmic to almost exclusive nuclear localization, and their levels of nucleolar occupancy displayed great differences (Figure 9F). Nucleolar accumulation of these isoforms was observed in response to proteotoxic stress or heat shock, whereas they assembled nucleolar cap-like structures following transcriptional arrest.

DISCUSSION

In this report, we have revealed an extensive repertoire of isoforms generated by processing of the human *RDM1* gene. Using primers designed to amplify alternatively spliced variants produced from two translation initiation sites, we have uncovered 11 cDNAs that are expressed in a variety of cell lines under normal growth conditions or in response to heat shock. While this manuscript was in preparation, an mRNA with a different 3'-untranslated region, which encodes a novel RDM1 isoform containing the first five exons of RDM1 α followed by a small, specific C-terminal extension was deposited in the NCBI database (accession number NM_001034836.1), adding to the complexity of this repertoire. The diversity of the RDM1 proteins lies in the presence or absence of sequences encoded by exon 1 and exons 4–7. Indeed, it is notable that, with the exception of RDM1 δ , all the RDM1 isoforms described to date contain exons 2 and 3. That the RDM1 proteins articulate around these two exons argues for their functional importance, as discussed below.

As a step to elucidating the function of the RDM1 proteins, we have examined the intracellular localization of RDM1 α and the other long N-terminal forms (containing exon 1). Our analysis has revealed a great diversity in the subcellular distribution patterns of these proteins. Thus, some variants were predominantly cytoplasmic, whereas others were almost exclusively nuclear. Likewise, great differences were seen in the nucleolar localization of these proteins. We suggest that the observed differences in subcellular distribution reflect functional differences among the RDM1 isoforms.

Our work has identified important determinants of the subcellular localization of the RDM1 proteins in the absence of stress. Exon 3, retained in all RDM1 isoforms, was found to contain nuclear and nucleolar targeting domains. Although NoLS and NLS signals remain to be delineated with precision within the 41-aa sequence of this exon, our data indicate that nucleolar accumulation of EGFP-tagged exon 3 was critically dependent upon the integrity of a small stretch of basic residues (R₉₈HK). NoLS, consisting of stretches of basic residues present in

single or multiple copies, have been identified in several nucleolar proteins and proposed to function by providing a protein-interaction interface with proteins that associate with the nucleolus (25,61, and references therein). Whether a similar mechanism applies to exon 3 remains to be determined. Substitution of AAA for R₉₈HK also decreased the overall levels of exon 3 in the nucleus, suggesting that these residues might be part of a NLS as well. Nuclear and nucleolar targeting domains were not restricted to exon 3 as a construct consisting of exons 1 + 2 was found to mediate the nuclear/nucleolar localization of EGFP, arguing for an important function of the RRM in the nucleus. Interestingly, the RRM domain localized less predominantly to the nucleolus than exon 3. The notion that both the RRM and exon 3 of RDM1 contribute functions in the nucleus raises the possibility of interplay between these domains. Studies of human La, a RRM-containing protein involved in the maturation of precursor RNAs located in the nucleoplasm or nucleolus, indicate that its intranuclear trafficking results from interplay between a functional NoLS and an RRM that is essential for its exit from the nucleolus (25). That a similar interplay operates between the NoLS of exon 3 and the RRM in some of the RDM1 proteins might explain the observed heterogeneity in nucleolar abundance of the RDM1 β isoform. Finally, our analyses so far have been limited to the long N-terminal isoforms. However, future studies of the short N-terminal RDM1 isoforms will be important since these forms lack exon 1 and thus the proposed RNP2 signature of the RRM. Others have shown that deletion of RNP2 in RRM1 or RRM2 of human La protein affected subnuclear localization (63). Whether the loss of exon 1 in the short N-terminal RDM1 isoforms affects the integrity and/or nucleic acid-binding properties of their RRM, as well as the determinants of its subcellular distribution, remains to be elucidated.

In addition to nuclear/nucleolar targeting domains, we have identified domains involved in the cytoplasmic retention of the RDM1 proteins. Comparison of the subcellular distribution patterns of RDM1 α and RDM1 γ indicates that one such domain is located in exon 5, as loss of this exon converts a predominantly cytoplasmic protein into a primarily nuclear one. Likewise, analysis of RDM1 δ suggests that sequences within exon 1 play a role in cytoplasmic retention by partially neutralizing the nuclear/nucleolar targeting functions of exon 3 to promote its cytoplasmic localization. References to cytoplasmic retention sequences are well documented in the literature (64–67). Based on these and other studies, several hypotheses can be made regarding the role of the cytoplasmic retention regions identified in RDM1 α . Firstly, they could mask potential nuclear localization signals located elsewhere in the protein, and require post-translational modification or conformational changes for these signals to be exposed in order to allow nuclear shuttling. Secondly, the cytoplasmic retention regions could shelter nuclear export signals. Although RDM1 α does not contain the classical leucine-rich nuclear export sequence (NES) found in the proteins exported by CRM1 (68), nor the M9- or KNS-types of NES

identified in hnRNPs (69,70), it is possible that it harbors a yet-unidentified NES. Finally, the cytoplasmic retention domains identified in this study could mediate important protein interactions or participate in substrate recognition in the cytoplasm. Since RDM1 α is predominantly cytoplasmic, it is therefore possible that its major partners/targets reside primarily in the cytoplasm. We propose that its cytoplasmic retention domains allow RDM1 α to fulfil RNA-binding activities in the cytoplasm. In support of this notion, preliminary analyses of immunopurified RDM1 α complexes have identified cytoplasmic as well as nuclear RNAs associated with RDM1 α (Van Dyck *et al.*, unpublished data). The characterization of these RNAs should illuminate the biological role of RDM1 α in RNA metabolism.

Some RDM1 isoforms localized to the nucleolus in the absence of stress, arguing for a function within this nuclear organelle. Moreover, RDM1 α and the long N-terminal isoforms accumulated in the nucleolus in response to certain stresses. The nucleolus assembles around the clusters of rDNA repeats and its primary function is to host ribosome biogenesis, including rDNA transcription, rRNA processing and pre-ribosome assembly. In addition to the factors involved in these reactions, the nucleolus also hosts hundreds of proteins from many functional classes that associate with the nucleolus in a dynamic manner (71). It is now well documented that the nucleolus plays an important role in stress responses (72), and a growing list of proteins have been shown to be excluded from or accumulate in the nucleolus in response to various forms of stress such as DNA damage (73), inhibition of transcription (71), proteasome inhibition (32,72) and heat shock (32). The evidence suggests that stress-induced nucleolar sequestration or release of a protein can serve as a mechanism to regulate protein function (72). The nucleolus can also function as a reservoir for unfolded proteins transported by molecular chaperones in an attempt to prevent damage to other nuclear compartments (74). It has also been proposed that nucleolar accumulation induced by inhibition of the proteasome reflects the stabilization of high-turnover proteins normally targeted for degradation in the nucleolus (61). To date, however, it has not been possible to detect the 26S proteasome in nucleoli (46, and references therein). In this study, nucleolar recruitment of the RDM1 isoforms was observed in response to three forms of stress that significantly alter the architecture of the nucleolus and its functions in rRNA transcription and/or processing; proteasomal inhibition (46), heat shock (75) and transcriptional arrest (34). The partial association of RDM1 α with nucleolar RNA in MG132-treated cell suggests that the targets of RDM1 α might include rRNAs or precursor rRNAs. Such association, however, did not require the proposed nucleic acid-binding domains of RDM1, indicating that it is mediated at least in part by protein-protein interactions. Similarly, the presence of RDM1 isoforms in nucleolar caps following transcriptional arrest may reflect the existence of newly exposed RNA and/or protein partners.

In this study, we found that chicken DT40 RDM1^{-/-} cells were more sensitive than wt cells to a heat shock

carried out at 45°C. RDM1 was dispensable for cell survival after exposure to MG132, suggesting functional redundancy in the mechanisms that operate in response to proteasome inhibition or that RDM1 is specifically required during the heat-shock response. We have previously reported that disruption of RDM1 in chicken DT40 cells conferred increased sensitivity to cisplatin (27). *In vitro*, chicken RDM1 protein interacted with ss- and dsDNA as well as RNA, and also recognized cisplatin-DNA lesions, leading us to propose several direct or indirect mechanisms by which RDM1 could modulate the cell response to cisplatin (27,28). Whether there is a functional link between the cisplatin- and heat-shock sensitive phenotypes of RDM1 null cells is currently unknown. Because physical agents and various chemicals that cause DNA damage can induce the expression of heat-shock proteins (HSPs), and since certain HSPs have been proposed to play a role in DNA repair and genomic stability (76,77, and references therein), it is possible that RDM1 impacts on DNA repair by modulating the expression and/or activity of HSPs. However, studies with Ehrlich ascites tumor cells have shown that cisplatin does not elicit a general stress response, inducing instead the expression of the small heat-shock protein Hsp25 via a transcription-independent mechanism (78). Others have shown that multidrug resistance can be induced by mechanisms dependent upon heat-shock factors (79, and references therein), and it is therefore also possible that the cisplatin-sensitive phenotype of RDM1 null cells results from dysfunction of these factors in the absence of RDM1. Finally, our data suggest that RDM1 plays a role in the cell response to extremely high temperatures in chicken cells. Avians present relatively high physiological temperatures compared with mammals, and functional differences have been observed between the heat-shock factors that mediate survival at high temperatures in avians and mammals. For instance, the functions fulfilled by human HSF1 are distributed in chicken cells between HSF1 and an avian-specific factor called HSF3, which is required for resistance to extremely high temperatures (59, and references therein). Thus, it will be important to determine whether and how the heat-shock sensitive phenotype of the chicken RDM1 null cells relates to the subcellular redistribution and nucleolar accumulation of the human RDM1 proteins as well as the up-regulation of some human RDM1 isoforms seen after mild heat shock.

SUPPLEMENTARY DATA

Supplementary Data are available at NAR Online.

ACKNOWLEDGEMENTS

This study was funded by La Ligue contre le Cancer, Comité du Rhône, France; Association pour la Recherche sur le Cancer, France. We are very grateful to Dr Young-Tae Chang (New York University) for his generous gift of the RNA-dye F22, Dr Yaron Shav-Tal (Bar Ilan University) for his comments on our analysis of nucleolar

caps and Marie Béatrice Secretan for her contribution during the early phase of this project. We thank Bakary Sylla and Birke Bartosch for critically reading the manuscript and Georges Mollon and Roland Dray for assistance during preparation of the Figures. Funding to pay the Open Access publication charges for this article was provided by the IARC regular budget.

Conflict of interest statement. None declared.

REFERENCES

- Maris,C., Dominguez,C. and Allain,F.H. (2005) The RNA recognition motif, a plastic RNA-binding platform to regulate post-transcriptional gene expression. *FEBS J.*, **272**, 2118–2131.
- Ishikawa,F., Matunis,M.J., Dreyfuss,G. and Cech,T.R. (1993) Nuclear proteins that bind the pre-mRNA 3' splice site sequence r(UUAG/G) and the human telomeric DNA sequence d(TTAGGG)n. *Mol. Cell. Biol.*, **13**, 4301–4310.
- Moran-Jones,K., Wayman,L., Kennedy,D.D., Reddel,R.R., Sara,S., Snee,M.J. and Smith,R. (2005) hnRNP A2, a potential ssDNA/RNA molecular adapter at the telomere. *Nucleic Acids Res.*, **33**, 486–496.
- Suswam,E.A., Li,Y.Y., Mahtani,H. and King,P.H. (2005) Novel DNA-binding properties of the RNA-binding protein TIAR. *Nucleic Acids Res.*, **33**, 4507–4518.
- Basu,A., Dong,B., Krainer,A.R. and Howe,C.C. (1997) The intracisternal A-particle proximal enhancer-binding protein activates transcription and is identical to the RNA- and DNA-binding protein p54nrb/NonO. *Mol. Cell. Biol.*, **17**, 677–686.
- DeAngelo,D.J., DeFalco,J., Rybacki,L. and Childs,G. (1995) The embryonic enhancer-binding protein SSAP contains a novel DNA-binding domain which has homology to several RNA-binding proteins. *Mol. Cell. Biol.*, **15**, 1254–1264.
- Johnston,S.D., Lew,J.E. and Berman,J. (1999) Gbp1p, a protein with RNA recognition motifs, binds single-stranded telomeric DNA and changes its binding specificity upon dimerization. *Mol. Cell. Biol.*, **19**, 923–933.
- Newberry,E.P., Latifi,T. and Towler,D.A. (1999) The RRM domain of MINT, a novel Msx2 binding protein, recognizes and regulates the rat osteocalcin promoter. *Biochemistry*, **38**, 10678–10690.
- Elantak,L., Tzakos,A.G., Locker,N. and Lukavsky,P.J. (2006) Structure of eIF3b-RRM and its interaction with eIF3j: structural insights into the recruitment of eIF3b to the 40S ribosomal subunit. *J. Biol. Chem.*, **282**, 8165–8174.
- Kielkopf,C.L., Lucke,S. and Green,M.R. (2004) U2AF homology motifs: protein recognition in the RRM world. *Genes Dev.*, **18**, 1513–1526.
- Fu,X.D. (1995) The superfamily of arginine/serine-rich splicing factors. *RNA*, **1**, 663–680.
- Graveley,B.R. (2000) Sorting out the complexity of SR protein functions. *RNA*, **6**, 1197–1211.
- Bouvet,P., Diaz,J.J., Kindbeiter,K., Madjar,J.J. and Amalric,F. (1998) Nucleolin interacts with several ribosomal proteins through its RGG domain. *J. Biol. Chem.*, **273**, 19025–19029.
- Kiledjian,M. and Dreyfuss,G. (1992) Primary structure and binding activity of the hnRNP U protein: binding RNA through RGG box. *EMBO J.*, **11**, 2655–2664.
- McBride,A.E., Cook,J.T., Stemmler,E.A., Rutledge,K.L., McGrath,K.A. and Rubens,J.A. (2005) Arginine methylation of yeast mRNA-binding protein Npl3 directly affects its function, nuclear export, and intranuclear protein interactions. *J. Biol. Chem.*, **280**, 30888–30898.
- Kzhyshkowska,J., Schutt,H., Liss,M., Kremmer,E., Stauber,R., Wolf,H. and Dobner,T. (2001) Heterogeneous nuclear ribonucleoprotein E1B-AP5 is methylated in its Arg-Gly-Gly (RGG) box and interacts with human arginine methyltransferase HRMT1L1. *Biochem. J.*, **358**, 305–314.
- Shen,H., Kan,J.L. and Green,M.R. (2004) Arginine-serine-rich domains bound at splicing enhancers contact the branchpoint to promote pre-spliceosome assembly. *Mol. Cell*, **13**, 367–376.
- Caceres,J.F., Misteli,T., Sreaton,G.R., Spector,D.L. and Krainer,A.R. (1997) Role of the modular domains of SR proteins in subnuclear localization and alternative splicing specificity. *J. Cell Biol.*, **138**, 225–238.
- Nichols,R.C., Wang,X.W., Tang,J., Hamilton,B.J., High,F.A., Herschman,H.R. and Rigby,W.F. (2000) The RGG domain in hnRNP A2 affects subcellular localization. *Exp. Cell Res.*, **256**, 522–532.
- Li,H. and Bingham,P.M. (1991) Arginine/serine-rich domains of the su(wa) and tra RNA processing regulators target proteins to a subnuclear compartment implicated in splicing. *Cell*, **67**, 335–342.
- Lai,M.C., Lin,R.I. and Tarn,W.Y. (2001) Transportin-SR2 mediates nuclear import of phosphorylated SR proteins. *Proc. Natl Acad. Sci. USA.*, **98**, 10154–10159.
- Kataoka,N., Bachorik,J.L. and Dreyfuss,G. (1999) Transportin-SR, a nuclear import receptor for SR proteins. *J. Cell Biol.*, **145**, 1145–1152.
- Helbig,R. and Fackelmayer,F.O. (2003) Scaffold attachment factor A (SAF-A) is concentrated in inactive X chromosome territories through its RGG domain. *Chromosoma*, **112**, 173–182.
- Allemand,E., Dokudovskaya,S., Bordonne,R. and Tazi,J. (2002) A conserved *Drosophila* transportin-serine/arginine-rich (SR) protein permits nuclear import of *Drosophila* SR protein splicing factors and their antagonist repressor splicing factor 1. *Mol. Biol. Cell*, **13**, 2436–2447.
- Horke,S., Reumann,K., Schweizer,M., Will,H. and Heise,T. (2004) Nuclear trafficking of La protein depends on a newly identified nucleolar localization signal and the ability to bind RNA. *J. Biol. Chem.*, **279**, 26563–26570.
- Fan,X.C. and Steitz,J.A. (1998) HNS, a nuclear-cytoplasmic shuttling sequence in HuR. *Proc. Natl Acad. Sci. USA*, **95**, 15293–15298.
- Hamimes,S., Arakawa,H., Stasiak,A.Z., Kierzek,A.M., Hirano,S., Yang,Y.G., Takata,M., Stasiak,A., Buerstedde,J.M. et al. (2005) RDM1, a novel RNA recognition motif (RRM)-containing protein involved in the cell response to cisplatin in vertebrates. *J. Biol. Chem.*, **280**, 9225–9235.
- Hamimes,S., Bourgeon,D., Stasiak,A.Z., Stasiak,A. and Van Dyck,E. (2006) Nucleic acid-binding properties of the RRM-containing protein RDM1. *Biochem. Biophys. Res. Commun.*, **344**, 87–94.
- Lloyd,J.A., McGrew,D.A. and Knight,K.L. (2005) Identification of residues important for DNA binding in the full-length human Rad52 protein. *J. Mol. Biol.*, **345**, 239–249.
- Campbell,R.E., Tour,O., Palmer,A.E., Steinbach,P.A., Baird,G.S., Zacharias,D.A. and Tsien,R.Y. (2002) A monomeric red fluorescent protein. *Proc. Natl Acad. Sci. USA*, **99**, 7877–7882.
- Dundr,M., Misteli,T. and Olson,M.O. (2000) The dynamics of postmitotic reassembly of the nucleolus. *J. Cell Biol.*, **150**, 433–446.
- Chatterjee,T.K. and Fisher,R.A. (2003) Mild heat and proteotoxic stress promote unique subcellular trafficking and nucleolar accumulation of RGS6 and other RGS proteins. Role of the RGS domain in stress-induced trafficking of RGS proteins. *J. Biol. Chem.*, **278**, 30272–30282.
- Philimonenko,V.V., Zhao,J., Iben,S., Dingova,H., Kysela,K., Kahle,M., Zentgraf,H., Hofmann,W.A., de Lanerolle,P. et al. (2004) Nuclear actin and myosin I are required for RNA polymerase I transcription. *Nat. Cell Biol.*, **6**, 1165–1172.
- Shav-Tal,Y., Blechman,J., Darzacq,X., Montagna,C., Dye,B.T., Patton,J.G., Singer,R.H. and Zipori,D. (2005) Dynamic sorting of nuclear components into distinct nucleolar caps during transcriptional inhibition. *Mol. Biol. Cell*, **16**, 2395–2413.
- Xie,S.Q., Martin,S., Guillot,P.V., Bentley,D.L. and Pombo,A. (2006) Splicing speckles are not reservoirs of RNA polymerase II, but contain an inactive form, phosphorylated on serine² residues of the C-terminal domain. *Mol. Biol. Cell*, **17**, 1723–1733.
- Arakawa,H., Hauschild,J. and Buerstedde,J.M. (2002) Requirement of the activation-induced deaminase (AID) gene for immunoglobulin gene conversion. *Science*, **295**, 1301–1306.
- Li,Q., Kim,Y., Namm,J., Kulkarni,A., Rosania,G.R., Ahn,Y.H. and Chang,Y.T. (2006) RNA-selective, live cell imaging probes for studying nuclear structure and function. *Chem. Biol.*, **13**, 615–623.

38. Fornerod, M., Ohno, M., Yoshida, M. and Mattaj, J.W. (1997) CRM1 is an export receptor for leucine-rich nuclear export signals. *Cell*, **90**, 1051–1060.
39. Engel, K., Kotlyarov, A. and Gaestel, M. (1998) Leptomycin B-sensitive nuclear export of MAPKAP kinase 2 is regulated by phosphorylation. *EMBO J.*, **17**, 3363–3371.
40. Rock, K.L., Gramm, C., Rothstein, L., Clark, K., Stein, R., Dick, L., Hwang, D. and Goldberg, A.L. (1994) Inhibitors of the proteasome block the degradation of most cell proteins and the generation of peptides presented on MHC class I molecules. *Cell*, **78**, 761–771.
41. Lee, D.H. and Goldberg, A.L. (1998) Proteasome inhibitors: valuable new tools for cell biologists. *Trends Cell Biol.*, **8**, 397–403.
42. Fenteany, G., Standaert, R.F., Lane, W.S., Choi, S., Corey, E.J. and Schreiber, S.L. (1995) Inhibition of proteasome activities and subunit-specific amino-terminal threonine modification by lactacystin. *Science*, **268**, 726–731.
43. Ginisty, H., Sicard, H., Roger, B. and Bouvet, P. (1999) Structure and functions of nucleolin. *J. Cell Sci.*, **112**, 761–772.
44. Ochs, R.L., Lischwe, M.A., Spohn, W.H. and Busch, H. (1985) Fibrillarin: a new protein of the nucleolus identified by autoimmune sera. *Biol. Cell*, **54**, 123–133.
45. Tollervey, D., Lehtonen, H., Jansen, R., Kern, H. and Hurt, E.C. (1993) Temperature-sensitive mutations demonstrate roles for yeast fibrillarin in pre-rRNA processing, pre-rRNA methylation, and ribosome assembly. *Cell*, **72**, 443–457.
46. Stavreva, D.A., Kawasaki, M., Dundr, M., Koberna, K., Muller, W.G., Tsujimura-Takahashi, T., Komatsu, W., Hayano, T. et al. (2006) Potential roles for ubiquitin and the proteasome during ribosome biogenesis. *Mol. Cell Biol.*, **26**, 5131–5145.
47. Borden, K.L. (2002) Pondering the promyelocytic leukemia protein (PML) puzzle: possible functions for PML nuclear bodies. *Mol. Cell Biol.*, **22**, 5259–5269.
48. Dellaire, G. and Bazett-Jones, D.P. (2004) PML nuclear bodies: dynamic sensors of DNA damage and cellular stress. *Bioessays*, **26**, 963–977.
49. Block, G.J., Eskiw, C.H., Dellaire, G. and Bazett-Jones, D.P. (2006) Transcriptional regulation is affected by subnuclear targeting of reporter plasmids to PML nuclear bodies. *Mol. Cell Biol.*, **26**, 8814–8825.
50. Wang, J., Shiels, C., Sasieni, P., Wu, P.J., Islam, S.A., Freemont, P.S. and Sheer, D. (2004) Promyelocytic leukemia nuclear bodies associate with transcriptionally active genomic regions. *J. Cell Biol.*, **164**, 515–526.
51. Luciani, J.J., Depetris, D., Usson, Y., Metzler-Guillemain, C., Mignon-Ravix, C., Mitchell, M.J., Megarbane, A., Sarda, P., Sirma, H. et al. (2006) PML nuclear bodies are highly organised DNA-protein structures with a function in heterochromatin remodelling at the G2 phase. *J. Cell Sci.*, **119**, 2518–2531.
52. Mattsson, K., Pokrovskaja, K., Kiss, C., Klein, G. and Szekely, L. (2001) Proteins associated with the promyelocytic leukemia gene product (PML)-containing nuclear body move to the nucleolus upon inhibition of proteasome-dependent protein degradation. *Proc. Natl Acad. Sci. USA*, **98**, 1012–1017.
53. Cioce, M. and Lamond, A.I. (2005) Cajal bodies: a long history of discovery. *Annu. Rev. Cell Dev. Biol.*, **21**, 105–131.
54. Morimoto, R.I. (1998) Regulation of the heat shock transcriptional response: cross talk between a family of heat shock factors, molecular chaperones, and negative regulators. *Genes Dev.*, **12**, 3788–3796.
55. Jordan, P., Mannervik, M., Tora, L. and Carmo-Fonseca, M. (1996) In vivo evidence that TATA-binding protein/SL1 colocalizes with UBF and RNA polymerase I when rRNA synthesis is either active or inactive. *J. Cell Biol.*, **133**, 225–234.
56. Reynolds, R.C., Montgomery, P.O. and Hughes, B. (1964) Nucleolar “caps” produced by actinomycin D. *Cancer Res.*, **24**, 1269–1277.
57. Haaf, T. and Ward, D.C. (1996) Inhibition of RNA polymerase II transcription causes chromatin decondensation, loss of nucleolar structure, and dispersion of chromosomal domains. *Exp. Cell Res.*, **224**, 163–173.
58. Jordan, P. and Carmo-Fonseca, M. (1998) Cisplatin inhibits synthesis of ribosomal RNA in vivo. *Nucleic Acids Res.*, **26**, 2831–2836.
59. Inouye, S., Katsuki, K., Izu, H., Fujimoto, M., Sugahara, K., Yamada, S., Shinkai, Y., Oka, Y., Katoh, Y. et al. (2003) Activation of heat shock genes is not necessary for protection by heat shock transcription factor 1 against cell death due to a single exposure to high temperatures. *Mol. Cell Biol.*, **23**, 5882–5895.
60. Lange, A., Mills, R.E., Lange, C.J., Stewart, M., Devine, S.E. and Corbett, A.H. (2007) Classical nuclear localization signals: definition, function, and interaction with importin alpha. *J. Biol. Chem.*, **282**, 5101–5105.
61. Song, Z. and Wu, M. (2005) Identification of a novel nucleolar localization signal and a degradation signal in Survivin-deltaEx3: a potential link between nucleolus and protein degradation. *Oncogene*, **24**, 2723–2734.
62. Creancier, L., Prats, H., Zanibellato, C., Amalric, F. and Bugler, B. (1993) Determination of the functional domains involved in nucleolar targeting of nucleolin. *Mol. Biol. Cell*, **4**, 1239–1250.
63. Horke, S., Reumann, K., Schulze, C., Grosse, F. and Heise, T. (2004) The La motif and the RNA recognition motifs of human La autoantigen contribute individually to RNA recognition and subcellular localization. *J. Biol. Chem.*, **279**, 50302–50309.
64. Burack, W.R. and Shaw, A.S. (2005) Live Cell Imaging of ERK and MEK: simple binding equilibrium explains the regulated nucleocytoplasmic distribution of ERK. *J. Biol. Chem.*, **280**, 3832–3837.
65. Chatterjee, T.K., Liu, Z. and Fisher, R.A. (2003) Human RGS6 gene structure, complex alternative splicing, and role of N terminus and G protein gamma-subunit-like (GGL) domain in subcellular localization of RGS6 splice variants. *J. Biol. Chem.*, **278**, 30261–30271.
66. Xia, J. and Kemper, B. (2007) Subcellular trafficking signals of constitutive androstane receptor: evidence for a nuclear export signal in the DNA binding domain. *Drug Metab. Dispos.*, **35**, 1489–1494.
67. Kanno, Y., Suzuki, M., Miyazaki, Y., Matsuzaki, M., Nakahama, T., Kurose, K., Sawada, J. and Inouye, Y. (2007) Difference in nucleocytoplasmic shuttling sequences of rat and human constitutive active/androstane receptor. *Biochim. Biophys. Acta.*, **1773**, 934–944.
68. Pemberton, L.F. and Paschal, B.M. (2005) Mechanisms of receptor-mediated nuclear import and nuclear export. *Traffic*, **6**, 187–198.
69. Michael, W.M. (2000) Nucleocytoplasmic shuttling signals: two for the price of one. *Trends Cell Biol.*, **10**, 46–50.
70. Nakiely, S. and Dreyfuss, G. (1997) Nuclear export of proteins and RNAs. *Curr. Opin. Cell Biol.*, **9**, 420–429.
71. Andersen, J.S., Lam, Y.W., Leung, A.K., Ong, S.E., Lyon, C.E., Lamond, A.I. and Mann, M. (2005) Nucleolar proteome dynamics. *Nature*, **433**, 77–83.
72. Mayer, C. and Grummt, I. (2005) Cellular stress and nucleolar function. *Cell Cycle*, **4**, 1036–1038.
73. Scott, M., Boisvert, F.M., Vieyra, D., Johnston, R.N., Bazett-Jones, D.P. and Riabowol, K. (2001) UV induces nucleolar translocation of ING1 through two distinct nucleolar targeting sequences. *Nucleic Acids Res.*, **29**, 2052–2058.
74. Nollen, E.A., Salomons, F.A., Brunsting, J.F., Want, J.J., Sibon, O.C. and Kampinga, H.H. (2001) Dynamic changes in the localization of thermally unfolded nuclear proteins associated with chaperone-dependent protection. *Proc. Natl Acad. Sci. USA*, **98**, 12038–12043.
75. Welch, W.J. and Suhan, J.P. (1985) Cellular and biochemical events in mammalian cells during and after recovery from physiological stress. *J. Cell Biol.*, **101**, 1198–1211.
76. Pandita, T.K., Higashikubo, R. and Hunt, C.R. (2004) HSP70 and genomic stability. *Cell Cycle*, **3**, 591–592.
77. Calini, V., Urani, C. and Camatini, M. (2003) Overexpression of HSP70 is induced by ionizing radiation in C3H 10T1/2 cells and protects from DNA damage. *Toxicol. In Vitro*, **17**, 561–566.
78. Gotthardt, R., Neininger, A. and Gaestel, M. (1996) The anti-cancer drug cisplatin induces H25 in Ehrlich ascites tumor cells by a mechanism different from transcriptional stimulation influencing predominantly H25 translation. *Int. J. Cancer*, **66**, 790–795.
79. Tchénio, T., Havad, M., Martinez, L.A. and Dautry, F. (2006) Heat shock-independent induction of multidrug resistance by heat shock factor 1. *Mol. Cell Biol.*, **26**, 580–591.